

# A new global database of Mars impact craters $\geq 1$ km: 2. Global crater properties and regional variations of the simple-to-complex transition diameter

Stuart J. Robbins<sup>1</sup> and Brian M. Hynek<sup>1,2</sup>

Received 20 September 2011; revised 20 April 2012; accepted 23 April 2012; published 5 June 2012.

[1] We have generated a new, 384,343-entry global crater database of Mars, statistically complete for craters with diameters  $D \geq 1$  km. In this release, the database contains detailed morphologic and morphometric data for craters  $D \geq 3$  km (future releases will extend these to smaller diameters). With detailed topographic data for the largest crater database to-date, we analyzed crater depth-to-diameter ratios for simple and complex morphologies across various terrains and for the planet as a whole and investigated the simple-to-complex morphology transition. Our results are similar to those in the published literature, but we found a substantial terrain dependence of the simple-to-complex transition that occurs at  $\sim 11$ -km-diameter craters at high latitudes. This suggests a model that requires melting of volatiles during high-latitude crater formation that fill the crater during the modification phase but will still support the simple morphology to larger diameters. We also use this database to reexamine previously observed distributions and patterns to show its fidelity and to further explore other global relationships of fresh craters, those with central peaks, pits, and summit pits. We present the global distribution of craters with different types of ejecta and morphometric properties. Overall, this database is shown to be comparable to previous databases where there is overlap and to be useful in extending prior work into new regimes.

**Citation:** Robbins, S. J., and B. M. Hynek (2012), A new global database of Mars impact craters  $\geq 1$  km: 2. Global crater properties and regional variations of the simple-to-complex transition diameter, *J. Geophys. Res.*, *117*, E06001, doi:10.1029/2011JE003967.

## 1. Introduction

[2] Crater populations can inform a variety of investigations of planetary processes, surface properties, physics, and geology. Detailed investigations of these require data about craters' positions, diameters, depths, and morphologies. Prior detailed work has focused on deriving these for isolated regions of Mars and so a true, global study has not been done with the crater properties that modern data permit to be gathered and derived, though global analyses have been done before [e.g., *Strom et al.*, 1992]. To this end, we have compiled the largest planetary crater database that exists today. This Martian crater catalog contains 384,343 craters with diameters  $D \geq 1$  km; the primary imagery data source

was THEMIS Daytime IR mosaics at 233 m/pix and 100 m/pix scales [*Christensen et al.*, 2004; *Edwards et al.*, 2011] (CTX imagery [*Malin et al.*, 2007] was occasionally used to supplement at high northern latitudes). In a process described in *Robbins and Hynek* [2012], we classified and derived many dozen morphologic and morphometric descriptors for each crater. Measurements from the database that were used in this work are from THEMIS-based circle fits unless otherwise explicitly stated.

[3] To both illustrate the fidelity and utility of this work, we have reexamined many previous general trends and properties of Martian impact craters reported in the literature and take them to new regimes. The small crater distribution as well as locations of fresh craters is examined in section 2. Crater interior and ejecta morphology are examined in section 3, exploring the distribution of crater central peaks, central pits, summit pits, and both radial and cohesive layered ejecta. Section 4 addresses revision of Martian crater topographic properties with the new data; it shows that rim heights are  $\sim 2\times$  smaller than are found on the Moon. Sections 5 and 6 present detailed recalculations of the depth-to-diameter function for simple and complex craters and the simple-to-complex morphology transition. This is done

<sup>1</sup>Laboratory for Atmospheric and Space Physics, University of Colorado Boulder, Boulder, Colorado, USA.

<sup>2</sup>Department of Geological Sciences, University of Colorado Boulder, Boulder, Colorado, USA.

Corresponding author: S. J. Robbins, Laboratory for Atmospheric and Space Physics, University of Colorado at Boulder, UCB 600, Boulder, CO 80309, USA. (stuart.robbs@colorado.edu)

Copyright 2012 by the American Geophysical Union.  
0148-0227/12/2011JE003967

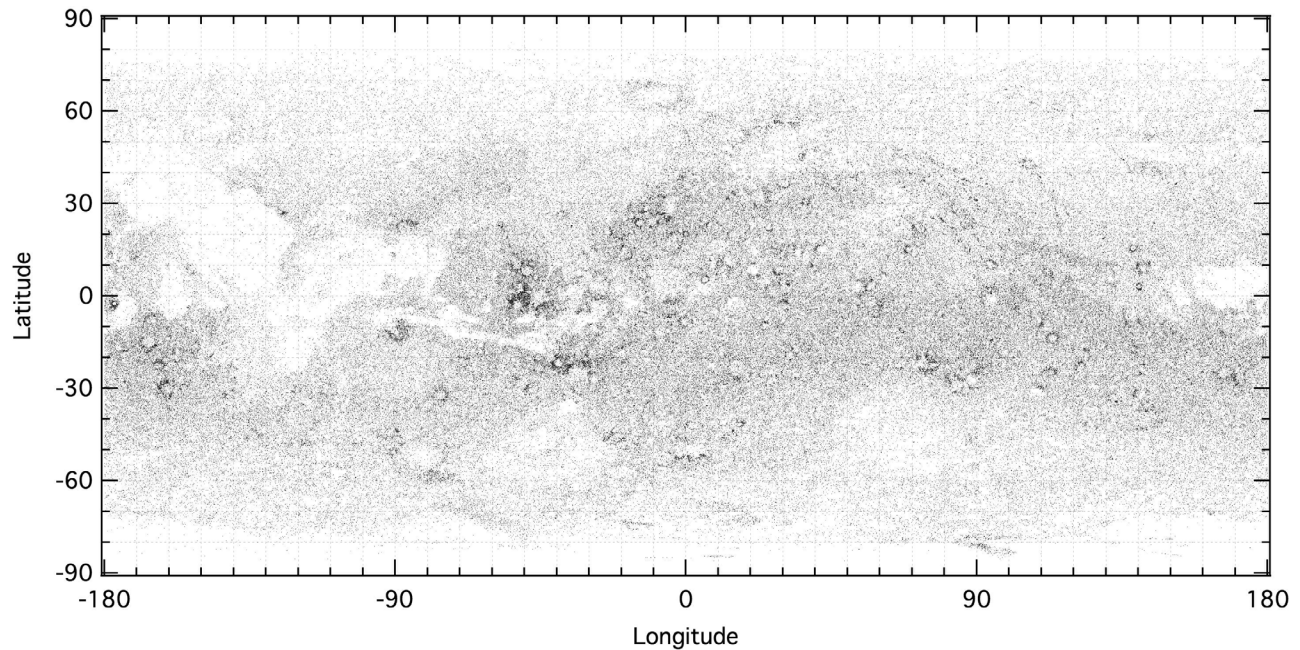


**Figure 1.** Locations of all  $1 \leq D < 3$  km craters on Mars included in this database, including potential secondary craters.

globally and by terrain that yielded disparate results discussed in section 7.

## 2. Global Crater Distributions

[4] The global crater distribution of Mars is generally well characterized in the literature, especially for larger (multikilometer) craters. Besides existing generalized crater databases [e.g., Barlow, 1988; Stepinski *et al.*, 2009; Salamunićcar *et al.*, 2011], global mapping efforts have identified large craters and used smaller craters to deduce stratigraphic relationships and ages [e.g., Scott and Tanaka, 1986; Tanaka, 1986; Greeley and Guest, 1987; Tanaka and Scott, 1987; Tanaka *et al.*, 2012]. In addition to global studies, regional or type studies have been completed, such as mapping craters on the poles [e.g., Banks *et al.*, 2010], mapping fresh craters [e.g., Boyce and Garbeil, 2007], identifying craters formed in the last few years [e.g., Byrne *et al.*, 2009; Daubar *et al.*, 2011] determining ages of major impact basins [Nimmo and Tanaka, 2005], and age-dating larger craters themselves [Werner, 2008]. What has not been previously shown is the global distribution of small, kilometer-scale impact craters, and this work is the first such study to address this issue.

### 2.1. Craters With Diameters Larger Than 3 km

[5] This database contains 79,723 craters with diameters  $D \geq 3.0$  km. Only two basins are included – Prometheus near the Martian South Pole, and Ladon near eastern Valles Marineris due to their clearly defined, if partial, rims. Other well known basins (such as Argyre, Hellas, or Utopia) or quasi-circular depressions [Frey, 2008, and references therein] were not included because their rims are more ambiguous and have been studied in much greater detail by

other researchers [e.g., Schultz *et al.*, 1982; Tanaka *et al.*, 2012]. The next-largest crater included is an unnamed 512-km-diameter crater, and there are 300 others that are  $D \geq 100$  km. Generally speaking, this database contains more craters larger than 100 km than other databases [Barlow, 1988; Stepinski *et al.*, 2009; Salamunićcar *et al.*, 2011], but not as many as found by Frey [2008]. Craters at smaller diameters ( $3 \leq D < 100$  km) are also approximately 10% more numerous than found in those databases [see Robbins and Hynes, 2012, section 7], which is likely due to use of the latest imagery in combination with global topography to identify craters.

### 2.2. Small Craters (1–3 km)

[6] The small,  $1 \leq D < 3$  km crater distribution on Mars is illustrated in Figure 1. The distribution of small craters can be used as a proxy for estimating relative regional ages where more craters indicate an older surface and fewer craters indicate a younger surface, though this is significantly complicated by local and regional resurfacing [Grant and Schultz, 1993; Tanaka, 2000]. Readily visible as young surfaces due to their relative paucity of craters are the major basins Argyre and Hellas, the Olympus Mons volcano and three Tharsis Montes, Elysium Basin, Valles Marineris, and both polar caps. More locally, there is clear contamination from secondary crater fields closely surrounding individual large primary craters such as Lomonosov ( $65.3^\circ\text{N}$ ,  $-9.3^\circ\text{E}$ ) and Oudemans ( $-9.8^\circ\text{N}$ ,  $-91.8^\circ\text{E}$ ) (see Robbins and Hynes [2011b] for a discussion of these fields). In addition, arcs of craters through Isidis are visible, likely emanating from Lyot crater ( $50.8^\circ\text{N}$ ,  $29.3^\circ\text{E}$ ), and these have been interpreted as secondary crater clusters from that large impact [Robbins and Hynes, 2011a].

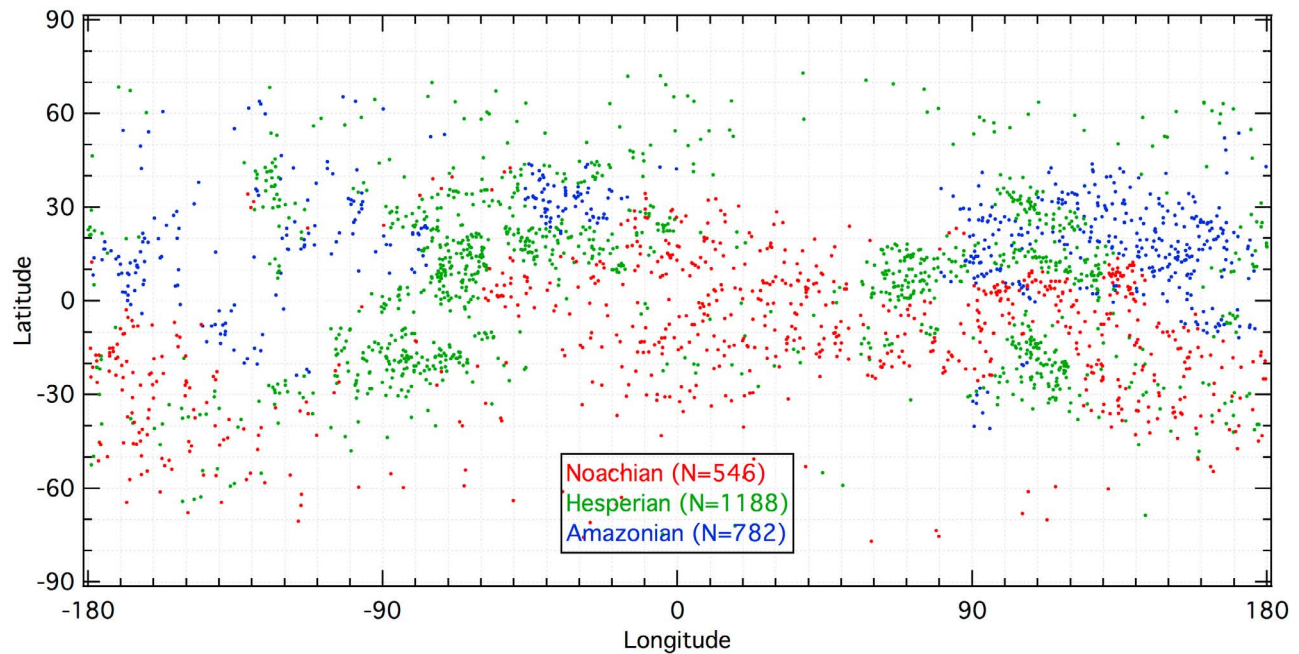


**Figure 2.** Scatterplot showing the distribution of all fresh  $D \geq 5$  km fresh craters. Fresh craters are generally concentrated close to the equator but show a larger latitude range centered at  $\sim 200^\circ\text{E}$ . Red dots represent craters on Noachian terrain, green are Hesperian, and blue are Amazonian. Terrain ages are from the Mars geologic maps [Scott and Tanaka, 1986; Greeley and Guest, 1987].

### 2.3. Fresh Craters

[7] Crater preservation/degradation/modification states were classified on a four-point scale. This was determined by examining each crater rim for sharpness and relief (1–4 pts), ejecta preservation (1–3 pts), floor infilling (1–4 pts), and relative depth/Diameter ratio (1–4 pts, determined based on latitude region; see section 5). Points were added and then scaled to a final 1–4 class where 1 was the most modified and 4 was a pristine or nearly pristine crater as viewed with 100 m/pix scale images. (See Robbins and Hynek [2012] for more detailed discussion of this system.)

[8] On an airless and geologically dead body, the distribution of fresh craters is nominally uniform over the surface since it should be of a uniform older age, though recent modeling work suggests a small latitude dependence based upon orbital mechanics may be present [Le Feuvre and Wieczorek, 2008]. On a body with an atmosphere and more recent geologic activity, such as Mars, the fresh crater distribution is instead a likely indicator of volcanic and aeolian erosion/modification efficiency across the planet [e.g., Greeley et al., 1992; Grant and Schultz, 1993] and periglacial processes on small craters near the poles. Figure 2 shows the global distribution of  $D \geq 5$  km fresh craters, and Figure 3 shows the percentage of fresh  $5 \leq D \leq 50$  km craters relative to all craters in that range. As a basic result, these show that erosion across the planet is far from uniform. Fresh craters are concentrated toward the equatorial regions and in specific mid- to high-northern latitudes (between  $\sim 100$ – $300^\circ\text{E}$ ). They are also more frequently found on younger terrain, as expected: Spatially, there are 14.5 fresh craters  $D \geq 5$  km per  $10^6$  km<sup>2</sup> of Noachian terrain, 24.8 for Hesperian, and 17.3 for Amazonian. More degraded craters are found at

the mid- to high-southern latitudes, agreeing well with the “softened” terrain of Mars that has been discussed previously in the literature [e.g., Jankowski and Squyres, 1992].

[9] The data show the greatest fractional concentrations of fresh craters (Figure 3) are centered around the major volcanic provinces (Tharsis, Elysium, and Syrtis Major) and the three basins Chryse, Isidis, and Utopia. A smaller concentration is also located between the two volcanoes Tyrrhena and Hadriaca Paterae. One can conclude from this that fresh craters are at least  $2\times$  more populous on younger terrain, especially volcanic, than most other surfaces. Volcanic terrain in general is stronger and so can better preserve these features. There is also a general abundance above the average in the mid- to high-northern latitudes that likely reflects their relative youth.

## 3. Crater Morphologies Across Mars

[10] Crater interior and ejecta morphologies are included in this release for craters  $D \geq 3$  km. The interior morphologic classifications include basic type (simple or complex) if it could be determined and notes of central peaks, central pits, and summit pits. Morphology descriptors of wall features such as terraces and secondary floor features such as faulting, channels, dunes, and other floor deposits are also noted. Ejecta morphologies and morphometries are detailed for Martian cohesive layered ejecta blankets. The general distributions and properties of crater morphologies are described in this section and compared with previous works.

### 3.1. Distribution of Central Peaks, Pits, and Summit Pits

[11] A classic feature of a fresh complex crater is a central peak, produced by rebound during the crater formation

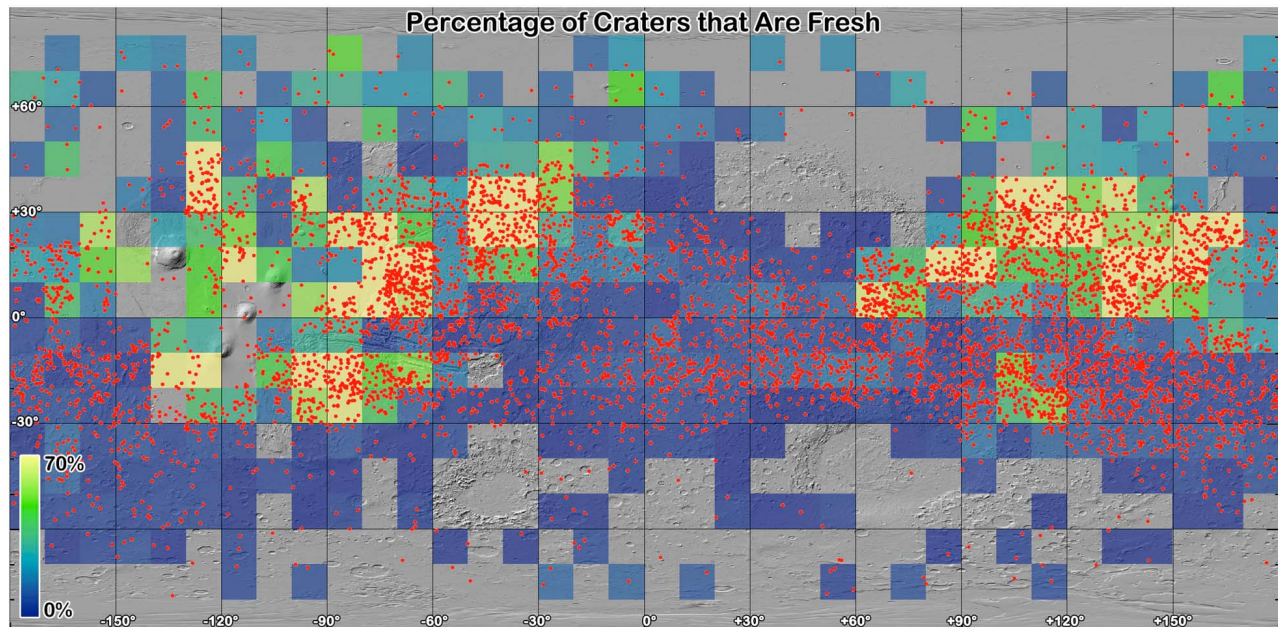


**Figure 3.** Area density plot showing the relative fraction of craters in  $10^\circ \times 10^\circ$  bins that are fresh versus the population of all 5–50-km-diameter craters. The raw craters are shown as red dots. Gaps are where there were not enough craters for an analysis or there were 0% fresh craters. Graticules are  $30^\circ$ .

process [e.g., Wood, 1973; Roddy, 1976]. Central peak craters number 3072 in this database. They represent a global average of  $\sim 6.3\%$  of all craters  $D \geq 15$  km, yet they comprise a disproportionate number of fresh craters ( $>90\%$  of fresh craters  $D \geq 15$  km contain central peaks). This likely indicates that many craters classified as “CpxFF” (complex, flat-floored) or “CpxUnc” (complex, unclassifiable) were originally central-peak craters but the peak has since been

buried or eroded and is now not detectable. This interpretation is supported by Figure 4 (the fraction of craters  $5 \leq D \leq 50$  km with central peaks) which clearly shows that central peak craters are generally present in a relatively even fraction throughout most of the planet.

[12] The data do show a noticeable deficit in a band of the southern highlands arcing from Argyre basin up to the equator at the prime meridian and back down through Hellas

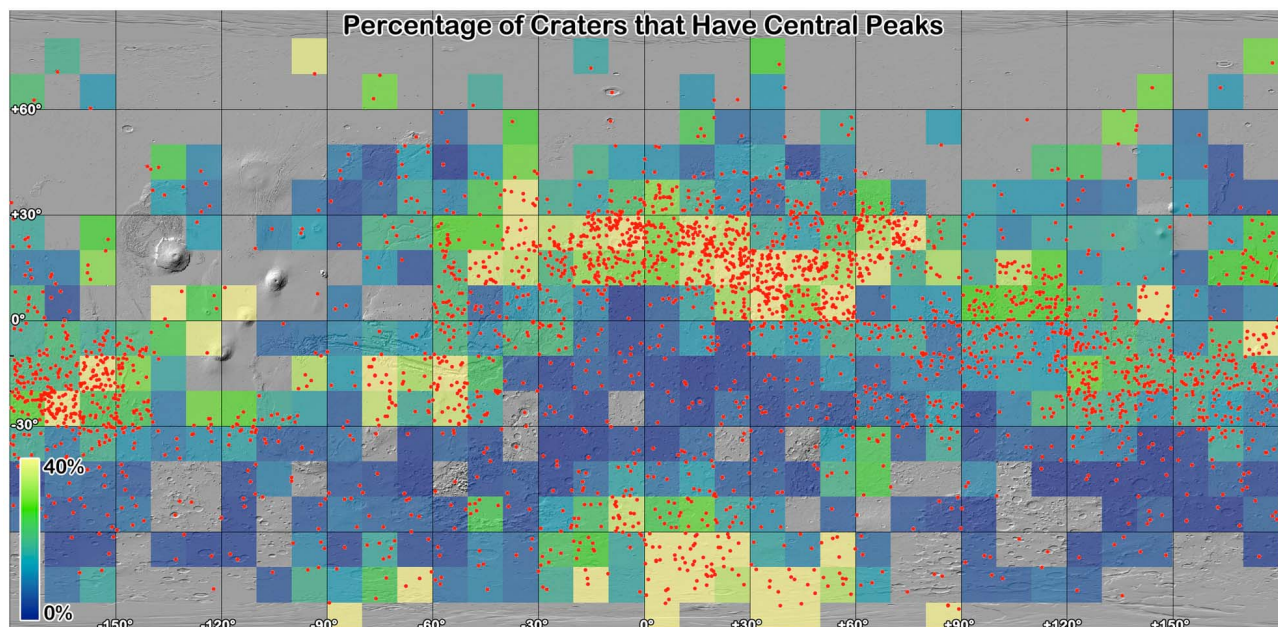


**Figure 4.** The fraction of craters  $5 \leq D \leq 50$  km in  $10^\circ \times 10^\circ$  bins that have central peaks. Underlying image is MOLA shaded relief. The raw craters are shown as red dots. Gaps are where there were no craters, graticules are  $30^\circ \times 30^\circ$ .

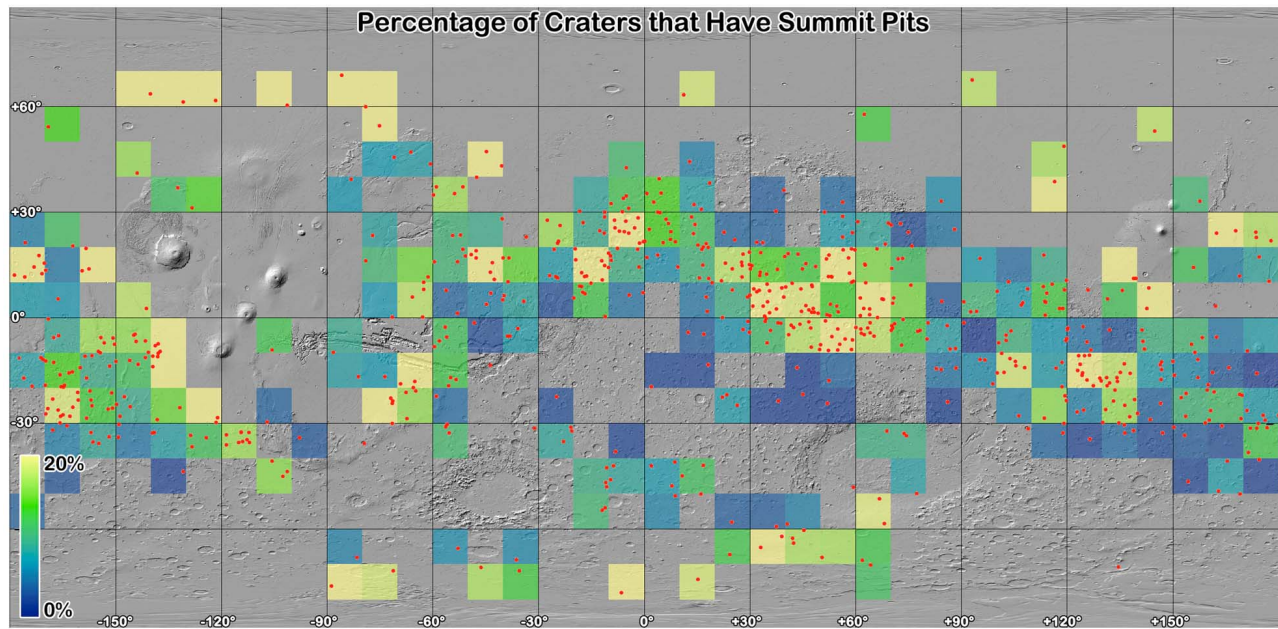


**Figure 5.** The fraction of craters  $5 \leq D \leq 50$  km in  $10^\circ \times 10^\circ$  bins that have summit pits. Underlying image is MOLA shaded relief. The raw craters are shown as red dots. Gaps are where there were no craters, graticules are  $30^\circ \times 30^\circ$ .

that does not correlate well with fresh craters (Figure 3). The fraction of central peaks is mildly enhanced in Arabia Terra and in the southern highlands south of  $\sim 60^\circ$ S and between East longitudes  $\sim -90^\circ$  to  $\sim 90^\circ$ . These suggest that this area has experienced enhanced erosion, in agreement with numerous previous studies that have indicated this area has experienced massive erosion, with suggested sources as polar wander [Schultz and Lutz, 1988; Tanaka, 2000] or running water [Hynek et al., 2002].

[13] A feature of some central peak craters on Mars is a pit in the middle of the peak to which a classification of “summit pit” is given [Barlow and Bradley, 1990]; these are also observed on the Moon and Mercury. Martian craters as well as those on Jupiter’s moons Ganymede and Europa also sometimes display central pits; these pits are occasionally observed in simple craters. Explanations for the genesis of these pits on crater floors or peaks are varied and include (1) vaporization of volatiles within the target during crater formation which releases gas near the center of the forming cavity [Wood et al., 1978; Senft and Stewart, 2008], (2) collapse of a central peak [Passey and Shoemaker, 1982], (3) excavation into layered target materials [Greeley et al., 1982], (4) a melt-drainage model whereby liquid produced near to and during the impact forms a transient lake in the crater center that subsequently drains into the subsurface, leaving behind a central pit [Croft, 1981; Bray et al., 2006; Alzate and Barlow, 2011], and/or (5) displacements related to the compression stage of crater formation [Schultz, 1988]. The percentages of craters with summit pits (672 craters) are shown in Figure 5, and the percentages with central pits (1841 craters) are shown in Figure 6.

[14] It is difficult to draw many conclusions from the distribution of summit pit craters because of the “small” numbers involved – despite this being the largest study ever done – though they do generally agree with findings by

Barlow [2011]: They are prevalent in Arabia Terra, southwest of Tharsis, and southwest of Elysium. They appear to correlate well with the distribution of central peaks. This would not be surprising if their genesis is of the collapse mechanism suggested by Passey and Shoemaker [1982]. However, there is a noticeable enhancement in the distribution north of Tharsis, and this is not observed in the central peak distribution. There is likely a cryosphere near the surface at higher northern latitudes [Boynton et al., 2002] that could indicate a volatile-dependent origin. However, the significance of this is questionable: In each bin at that latitude ( $60\text{--}70^\circ$ N), the number of craters with summit pits is 1.

[15] Central pit craters (Figure 6) are found to be enhanced relative to the global average around all volcanic centers, in general agreement with findings by Barlow [2011]: Tharsis, Elysium Syrtis Major, the Tyrrhena-Hadriaca corridor, and southwest of Hellas around Pityusa, Amphitrites, Peneus, and Malea Paterae. While these correlate with the fresh crater population, this is likely because the fresh craters correlate well with the volcanic terrain. There is also an enhancement near the prime meridian and in the range about  $0\text{--}30^\circ$ S latitude that is not related to volcanic landforms.

[16] Subsurface ice near the equatorial Martian latitudes is not stable unless obliquities are  $>27^\circ$ , and it is not stable in the Elysium region until obliquities are  $>30^\circ$  [Mellon and Jakosky, 1995]; if ice is present today near the equator, it is likely buried far below the surface [Clifford, 1993; Boynton et al., 2002]. If the evacuation into subsurface liquid water reservoirs were the formation mechanism of central pits on Mars, though, one would expect significant concentration of central pit craters near the poles; this is not observed. Even though Mars’ present-day obliquity is probably low compared with the long-term average, central pits are broadly concentrated in equatorial regions. This would require that the vast majority of these craters – which

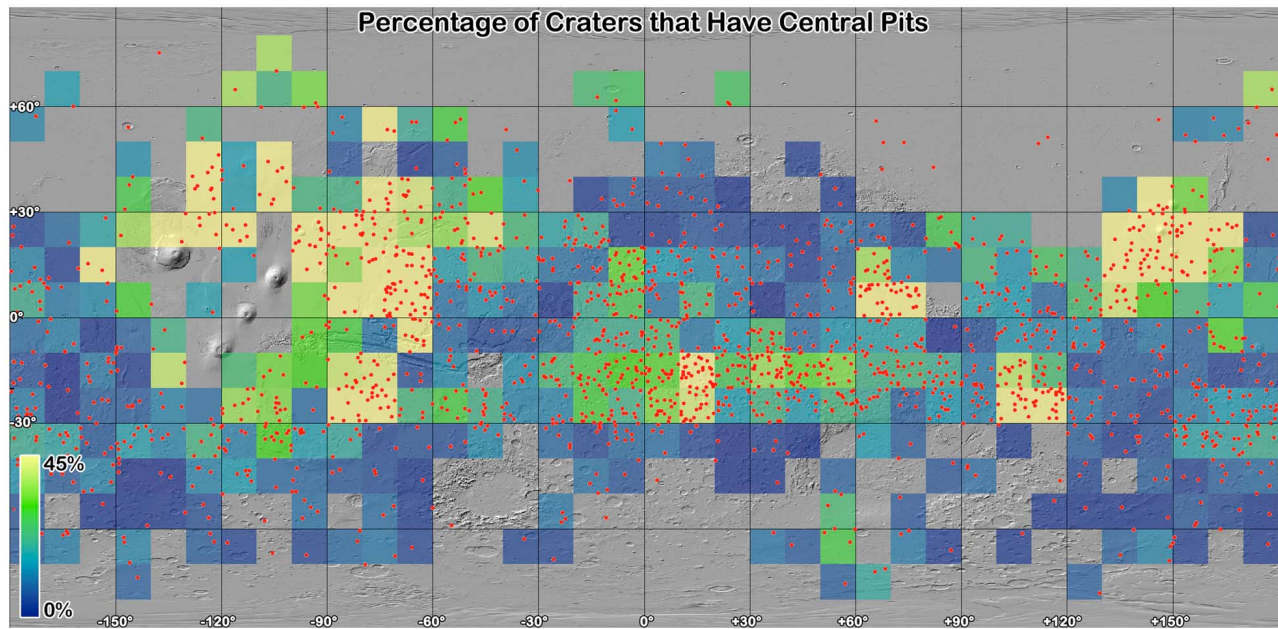


**Figure 6.** The fraction of craters  $5 \leq D \leq 50$  km in  $10^\circ \times 10^\circ$  bins that have central pits. Underlying image is MOLA shaded relief. The raw craters are shown as red dots. Gaps are where there were no craters, graticules are  $30^\circ \times 30^\circ$ .

are a non-trivial fraction of the overall craters - formed when obliquities were  $>60^\circ$ , which is fairly unlikely [Laskar *et al.*, 2004]. Similarly, central pit craters are generally among the fresh crater population (92% were a preservation state of 3 or 4), and they are missing in the high southern latitudes where central peaks were prevalent. Thus, they are likely not a collapse from a central peak. Of the five proposed mechanisms, none have predictions of the distribution of central pits that matches that in this database, though it is not possible to draw a prediction from the proposal in Schultz [1988]. The now-favored melt-drainage model in the literature [e.g., Alzate and Barlow, 2011] appears to be less likely given the distribution, though it cannot be ruled out.

[17] However, one must keep in mind that while these data do not support any of the four proposed mechanisms, it is entirely possible that the distribution is an artifact of preservation across the planet. With 92% of central pit craters being fairly fresh, and a topographic depression being the first to fill with any material, there is likely a significant observational bias. If there is any target- or geologic-related bias in their formation, at best it can be concluded that these are still an enigmatic feature with a formation that cannot be gleaned from a simple present-day global distribution approach.

### 3.2. Ejecta Morphologies

[18] Crater ejecta usually indicates youth, and on the Moon it is useful for geologic mapping and age relationships. On the Moon, craters display a radial ejecta morphology where the material has been ballistically emplaced during the excavation phase of crater formation as individual particles ejected during impacts. When probes returned the first images of Mars, a wholly new class of ejecta was observed. The terminology has varied significantly over the years (see discussion in Robbins and Hynek [2012]), but the

term “layered ejecta” is now part of the standardized nomenclature [Barlow *et al.*, 2000]. This database contains morphologic indications for ejecta and morphometric data for the layered type that are explored in brief in this section for craters  $D \geq 3$  km.

#### 3.2.1. Radial Ejecta

[19] Of the 79,723 craters  $D \geq 3$  km in this database, radial ejecta is the sole ejecta type in 24,897 craters (31.2%). A crater was considered to have radial ejecta if there appeared to be radial patterns radial to the rim; this could include eroded ejecta where all that remains are remnant patterns [Schultz, 1992]. The spatial density on each terrain type per  $10^6$  km<sup>2</sup> is: 161 Noachian, 54 Hesperian, and 23 Amazonian. It is clear from this that radial ejecta patterns on Mars can still be visible around ancient craters, otherwise the distribution should be even if one assumes craters form uniformly across the different terrain types. In fact, the relative densities are more disparate than those from the fresh crater population, as one would expect if this were the case.

#### 3.2.2. Layered Ejecta

[20] When Martian layered ejecta craters were first examined, it was thought they were part of a type evolution that started with multilayered craters that erode to single-layer ejecta craters that finally erode to pedestal craters [McCauley, 1973]. Woronow and Mutch [1980] and Mutch and Woronow [1980] were among the first to quantitatively examine the geometric properties of the ejecta of each and determine they are not evolutionarily related. Over the years, two hypotheses emerged and remained for a formation process of the layered ejecta. One holds that they are formed when an impactor hits a volatile-rich subsurface, the impact energy melts or vaporizes the volatiles, and the ejecta acts like a fluid as a result [e.g., Carr *et al.*, 1977]. The other states that they form when the severity of the impact causes atmospheric vortexes and winds [e.g., Schultz and Gault,

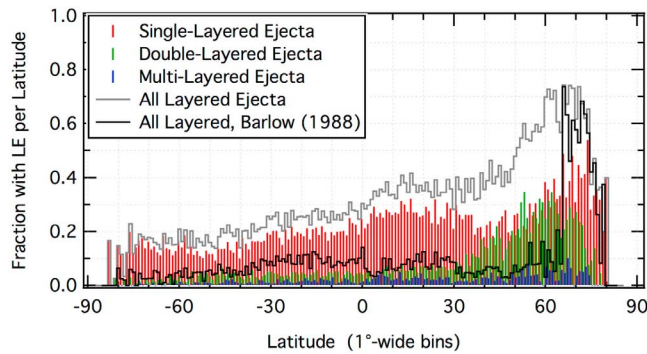


**Figure 7.** Distribution of layered ejecta craters, by type, per latitude bin for craters  $D \geq 5$  km (for fair comparison with *Barlow* [1988]). Red, green, and blue indicate SLE, DLE, and MLE distribution, respectively, while the gray line shows the sum of all three. For reference, the sum of all LE types from *Barlow* [1988] is shown as a black line.

1979; *Schultz*, 1992]. It is possible a combination of both models is at work on Mars [e.g., *Barlow*, 2005; *Komatsu et al.*, 2007].

[21] Over the years, these forms of ejecta have only been observed on Venus, Mars, Ganymede, and Europa [e.g., *Barlow et al.*, 2000; *Boyce et al.*, 2010]. The lack of atmosphere on Ganymede and Europa indicates that an atmosphere and hence the atmospheric vortex model may not be required for the formation of these kinds of ejecta, but the intense surface heat on Venus suggests that volatiles within the impact medium may also not be necessary in some formation situations. Determining the morphometric characteristics of each should help constrain these and discriminate between the two in different cases. Motivationally, if it can be shown that morphometric analysis required volatiles for the ejecta to form, then high concentrations of these crater types could indicate where subsurface water may be for future human exploration. To this end, an introduction to the distributions and characteristics is presented here, and future work will focus on combining these with mineralogic, thermal inertia, and crater age dating of the ejecta blankets themselves to distinguish between the models.

[22] Of the 79,723 craters  $D \geq 3$  km in this database, a total of 18,841 are surrounded by layered ejecta blankets: 14,679 are single-layered (SLE), 3333 are double (DLE), and 829 are multiple (three or more) (MLE). (See *Robbins and Hynes* [2012] for a detailed description of all ejecta morphologic and morphometric properties in the database.) The *Barlow* Database [*Barlow*, 1988] for craters  $D \geq 5$  km contains 3221, a factor of  $\sim 4\times$  fewer over the same diameter range for this database. There is a size dependence observed on the number of layers. The largest SLE crater is a 111-km-diameter crater, the largest DLE is 78 km, and largest MLE is 83 km. These could be considered outliers, though, and insignificant in determining the onset of these features because all types start to increase dramatically on a size-frequency diagram at  $D \sim 30\text{--}40$  km; they are statistically identical in frequency for  $D \geq 20$  km. For MLE, the peak in frequency is sharp at  $D = 17$  km; it is rarer for a crater to display MLE blankets at smaller diameters. The peak for DLE is at 12 km, and the peak for SLE craters is at approximately 5.3 km. Both DLE and SLE craters have

fairly constant numbers for diameters  $\sim 3\text{--}16$  km and  $\sim 3\text{--}7$  km, respectively, though these form a decreasing fraction of the overall craters at smaller diameters.

[23] These craters are not distributed uniformly across the planet, a feature that has been known for many years (and characterized, for example, in *Barlow* [1988]). When examining the latitude-dependence, Figure 7 clearly shows these craters are more numerous in the northern hemisphere and especially at high northern latitudes  $50^\circ\text{--}80^\circ\text{N}$ . The enhancement around  $10^\circ\text{N}$  is likely due to volcanic terrain abundance at this latitude, discussed below. *Barlow and Perez* [2003] and *Barlow* [2005] found a relatively even distribution across the planet with a marked spike  $\sim 65\text{--}80^\circ\text{N}$ . Another feature of the *Barlow* Database that this catalog reproduces well is the significant increase of DLE craters  $\sim 40\text{--}75^\circ\text{N}$  (though *Barlow and Perez* [2003] found a tighter latitude range).

[24] Expanding this distribution in longitude, Figure 8 shows all SLE, DLE, and MLE craters as a fraction of all craters within a  $5^\circ \times 5^\circ$  bin, similar to analyses in *Barlow and Perez* [2003] from Viking data. Clearly visible are several trends. First, SLE craters dominate all volcanic terrains (that have a significant number of craters on them). They also dominate in the high northern latitudes. DLE craters are similar though they clearly dominate at higher northern latitudes as indicated in Figure 7. In general, there was no longitude dependence upon the distribution of DLE craters, though there was a slight increase in the eastern Tharsis and lower Valles Marineris region. It is difficult to draw conclusions from the MLE distribution due to small numbers (even at coarser binning, global trends are not apparent). The most that can be confidently stated is that the MLE distribution does not disagree with the SLE distribution, and there is an enhancement around Elysium. These all agree with the general conclusions from *Barlow and Perez* [2003] with the main anomaly being the concentration of SLE craters to the southwest of Valles Marineris. This could be an artifact of the way the data are presented: In Figure 7, LE types are shown as a fraction of all craters, but in *Barlow and Perez* [2003], the data are discussed and displayed as a fraction of craters with ejecta.

[25] A morphometric characteristic examined is ejecta mobility, the extent to which the ejecta travels relative to the crater radius. This database uses the average extent, following *Barlow* [2005]. It reproduces those findings well, though the average ejecta mobility is a little less and the maximum extents were a little more in this work (see Table 1). An additional feature identified in early work [*Mouginis-Mark*, 1979] is a latitude dependence with ejecta mobility where, near the poles, the average is up to 2.0 versus the equatorial average of 1.4. This catalog's data show a similar trend with the transition happening at  $\sim \pm 30\text{--}40^\circ$ . Ranges poleward of  $\pm 40^\circ$  were examined separately from an equatorial region  $\pm 30^\circ$ , and values are reported in Table 1. Polar crater layered ejecta is found to travel farther than equatorial, while that in the northern hemisphere travels farther than in the south.

#### 4. Crater Shapes

[26] Basic crater shapes have been measured for decades [e.g., *Pike*, 1976], and this database provides the ability to

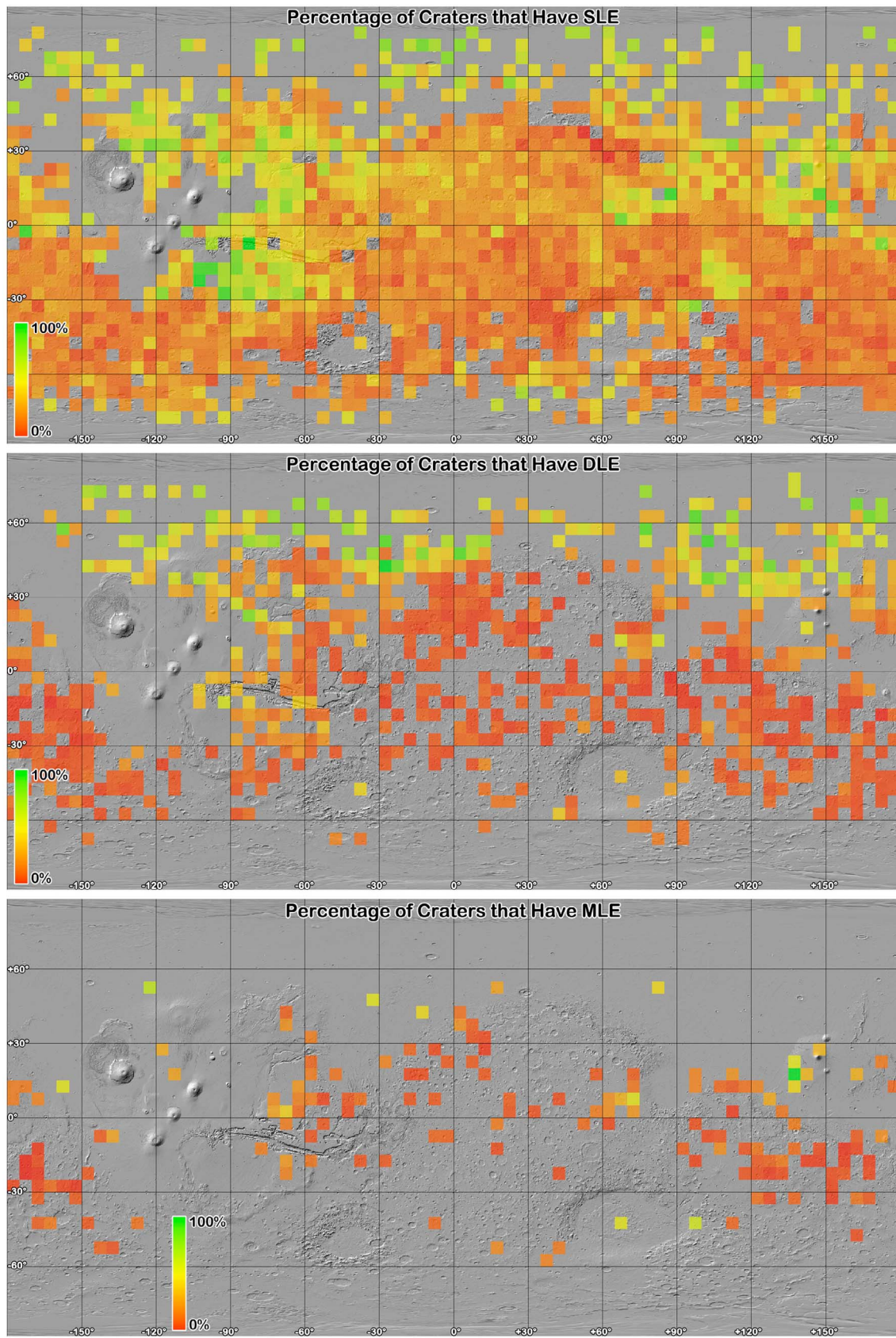


**Figure 8.** The fraction of craters  $5 \leq D \leq 50$  km in  $5^\circ \times 5^\circ$  bins that have layered ejecta blankets. Underlying image is MOLA shaded relief. Gaps are where there were  $\leq 1$  craters of any type per bin, graticules are  $30^\circ \times 30^\circ$ .

**Table 1.** Average Ejecta Mobility Values for Select Layered Ejecta Types<sup>a</sup>

	SLE	DLE Inner	DLE Outer
Global	1.4	1.4	2.5
<-40°N Latitude	1.6	1.5	2.5
±30° Latitude	1.2	1.2	1.8
>+40°N Latitude	2.0	1.5	3.2

<sup>a</sup>Units are crater radii.

verify and update these morphometric values on Mars. Only fresh craters  $D \geq 5$  km of preservation class 4 were used for this analysis (1964 simple and 1413 complex). This section addresses crater rims and surface-to-floor scaling, separate from scaling of crater depth (rim-floor) as a function of diameter which is described in section 5. Both of these rely upon accurate rim height measurements, a value that is in question given the relatively coarse nature of Mars Orbiter Laser Altimeter (MOLA) [Zuber *et al.*, 1992; Smith *et al.*, 2001] gridded data. The fidelity of measurements in this database was addressed in detail in Robbins and Hynek [2012], which found them to be reliable for these purposes: To within the uncertainty quoted in the database in rim heights, it was found that the measurements from gridded data were accurate when compared with the MOLA point data. In this database, extreme values were ignored: Rim, surrounding surface, and floor elevations were measured as the average of  $N$  topographic data points for each. Throughout this section, comparison data are from Pike [1976, 1977], Wood and Andersson [1978], and Hale and Head [1979] as summarized by Melosh [1989].

[27] The first feature often addressed is rim height above the surrounding surface. At a basic level, this scales with crater diameter, and generalized results based on lunar data show that rim height is  $\sim 4\%$  of the crater diameter. However, examination of the Martian craters in this database shows a well-defined Gaussian distribution of this relationship for simple craters  $1.9 \pm 0.7\%$  and  $1.4 \pm 0.6\%$  for complex craters. This rim height is  $>2\times$  smaller than what is typically reported. A possible explanation is that this database uses the average elevation around the crater rim instead of the highest point, but that is unlikely to be able to account for this large of a difference. Similarly, Melosh [1989] quotes from the above mentioned aggregated sources that the surface-to-floor depth of simple craters is  $\sim 20\%$  the crater diameter, but the simple craters in this database have a relationship of  $8.9 \pm 1.9\%$ . This is again  $>2\times$  smaller than what is typically reported. Complex craters are shallower with a surface-to-floor depth  $6.2 \pm 1.9\%$  the crater diameter.

[28] When looking at a diameter-dependence for rim height, apparently fresh craters were examined in the method detailed below for depth/Diameter relationships. For these simple craters, a power law  $h = 0.011D^{1.300}$  was fit, and a relationship of  $h = 0.025D^{0.820}$  was found for complex craters (where  $h$  is rim height and  $D$  is crater diameter). In contrast, in  $\sim 6000$  craters examined, Garvin *et al.* [2003] found  $h = 0.04D^{0.31}$  for simple craters (significantly different) but  $h = 0.02D^{0.84}$  for complex (statistically identical). Better topographic data for smaller-diameter craters should help determine which - if either - is accurate.

[29] Another way to examine scaling is to measure rim height relative to the overall rim-to-floor crater depth. This is

found to follow a Gaussian with a mean  $16 \pm 6\%$  for simple craters and  $18 \pm 6\%$  for complex craters. The similar values indicate that the uplift and overturn that results in rim formation scales well through these two crater morphologies.

## 5. Global Depth/Diameter Relationships

[30] The ratio of a crater's depth to its diameter is one of its most fundamental properties, but it is one that was not directly measurable for extraterrestrial craters until the last two decades. Prior, crater depths were estimated through photogrammetry and shadow lengths, processes that rely on knowing sun angles and the former assuming a uniform surface albedo [e.g., Chapman and Jones, 1977; Pike, 1976, 1977, 1980a, 1988; Davis and Soderblom, 1984]. With the inclusion of the MOLA instrument on Mars Orbiter, global laser altimetry data has allowed for the uniform measure of crater topographic properties provided in this database. These were measured from the MOLA gridded data (MEGDR) as described in Robbins and Hynek [2012]. Briefly, crater rims and floors were identified in MEGDR data and the average elevation of points along the rim and deepest sections of the floor were used to compute the rim-to-floor depth. This was found to be accurate when compared with the MOLA point data (PEDR), as limited random sampling performed in Robbins and Hynek [2012] suggests the recorded values are accurate to within the uncertainties that were also recorded. Future work comparing these data with the Mars Express's High-Resolution Stereo Camera (HRSC) [Neukum and Jaumann [2004] should clarify this, but at present the MOLA data are still used. Throughout this work, the "rim-to-floor" depths were used unless otherwise stated.

[31] Previous work by Garvin *et al.* [2003] estimated a  $d = 0.21D^{0.81}$  relationship for simple craters  $D \leq 6$  km, and  $d = 0.36D^{0.49}$  for complex craters  $D > 6$  km. Boyce and Garbeil [2007] find a similar curve of  $d = 0.315D^{0.52}$  for complex craters  $D \geq 7$  km. While hesitant to quote a global average for reasons discussed below, this database yields a simple crater relationship of  $d = 0.179D^{1.012}$  and a complex one of  $d = 0.286D^{0.582}$ ; these are comparable to previous works, though there is some variation as one may anticipate, as discussed below.

### 5.1. Regional Depth/Diameter Relationships

[32] Across the surface of a planetary body, one might expect the ratio of a crater's depth to diameter to be reasonably constant; on Mars, however, a fresh-looking crater's observed depth can vary significantly depending upon where it formed, as shown throughout this section. This affects any "global" depth/Diameter ratio ( $d/D$ ) one may quote, though this has been done throughout the literature for decades [e.g., Pike, 1980a; Garvin *et al.*, 2000, 2003; Boyce and Garbeil, 2007; Stepinski *et al.*, 2009]. To illustrate this, craters were separated by simple and complex morphologies and then into different diameter ranges. Diameter ranges within each morphology were done because there is no set ratio for the  $d/D$  value for fresh simple or complex craters - even though it is often quoted as 1:5 and 1:10-100, respectively [Pike, 1977; Melosh, 1989].

[33] All craters were divided into six diameter ranges that each encompassed roughly a factor of  $2\times$  in size. Smaller

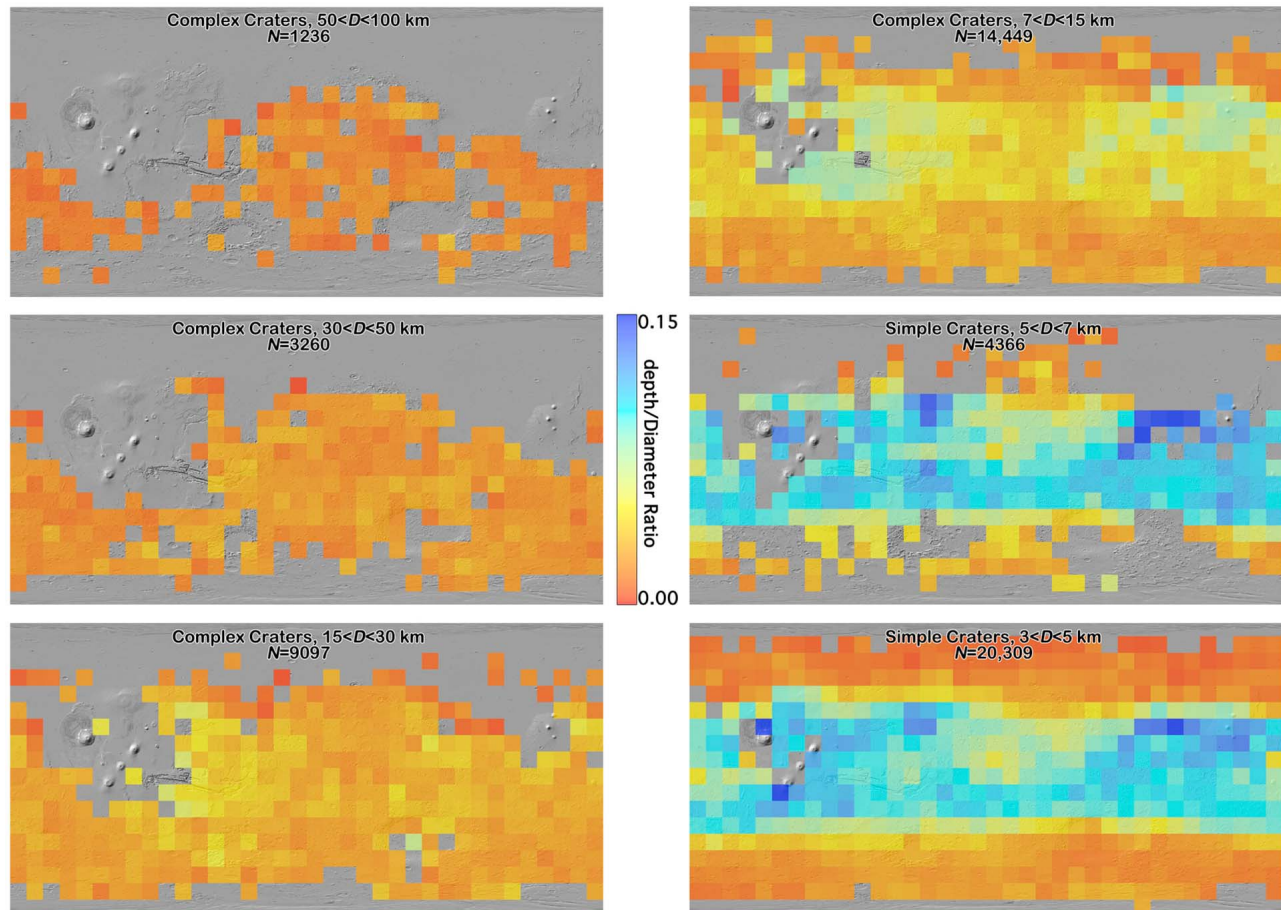


**Figure 9.** Six panels showing binned crater depth/Diameter ratios across Mars in  $10^\circ \times 10^\circ$  bins; bins with  $N < 5$  craters were removed. Four panels show complex craters and two are simple.

ranges had small-numbers problems that limited the overall utility, while larger ranges muted the differences and hence analysis that could be done. Simple craters were separated into two ranges – 3–5 km ( $N = 20,309$ ) and 5–7 km ( $N = 4366$ ). Complex craters were separated into four: 7–15 km ( $N = 14,449$ ), 15–30 km ( $N = 9097$ ), 30–50 km ( $N = 3260$ ), and 50–100 km ( $N = 1236$ ). Craters were then binned into  $10^\circ \times 10^\circ$  latitude/longitude bins and the mean  $d/D$  value was calculated; bins with  $< 5$  craters were removed. These are shown in Figure 9. A similar analysis was done for fresh craters only (preservation states 3 and 4), illustrated in Figure 10, in  $30^\circ \times 30^\circ$  bins. The results were comparable given the limitations, as discussed below.

[34] Readily apparent from Figure 9 is significant global variation. To first-order, craters  $D \gtrsim 20$  km poleward of  $\sim \pm 40^\circ$  latitude are significantly shallower than their counterparts closer to the equator by as much as a factor of 2–3 $\times$ . Second-order effects are that craters near the major volcanic complexes - Tharsis and Elysium - are deeper than the general average, and craters within the Isidis, Utopia, and northern Chryse/southern Acidalia impact basins are the deepest on the planet, on average. Similar results were observed by *Boyce et al.* [2006], except they did not identify this effect in northern Chryse (this was not in their study area). In the equatorial range, the shallowest craters are within Arabia Terra, unique from the southern highlands.

The patterns noted here disappear at larger crater diameters, or at least as far as can be determined from the smaller numbers. The last remnants of the pattern are in the 15–30 km range, showing deeper craters around Tharsis and Elysium and shallower craters toward the north pole, but not the south.  $D > 30$  km craters do not show this.

[35] Analysis of the relatively fresh crater population (preservation states 3 and 4) shown in Figure 10 support the majority of these observations: Craters are shallower near the equator and deeper near the poles, and this effect persists up to the  $D \leq 30$  km range. The more localized findings of deeper craters in the northern hemisphere basins is not found, though this is likely because of small number statistics; finer binning in the  $3 \leq D < 7$  km simple crater range removes bins over those regions due to small numbers, so the effects are averaged out at the coarser binning shown. Deeper craters at small diameters are observed over the Tharsis region, though. The shallower craters observed in Arabia Terra are not found at smaller diameters but are somewhat visible between 7 and 30 km, though the difference is slight. This overall agreement between Figures 9 and 10 support the interpretation that Figure 9 is generally indicative of the fresh crater population and the interpretations that follow.

[36] The equatorial/polar dichotomy disappearing for  $D > 30$  km craters can be interpreted as larger craters

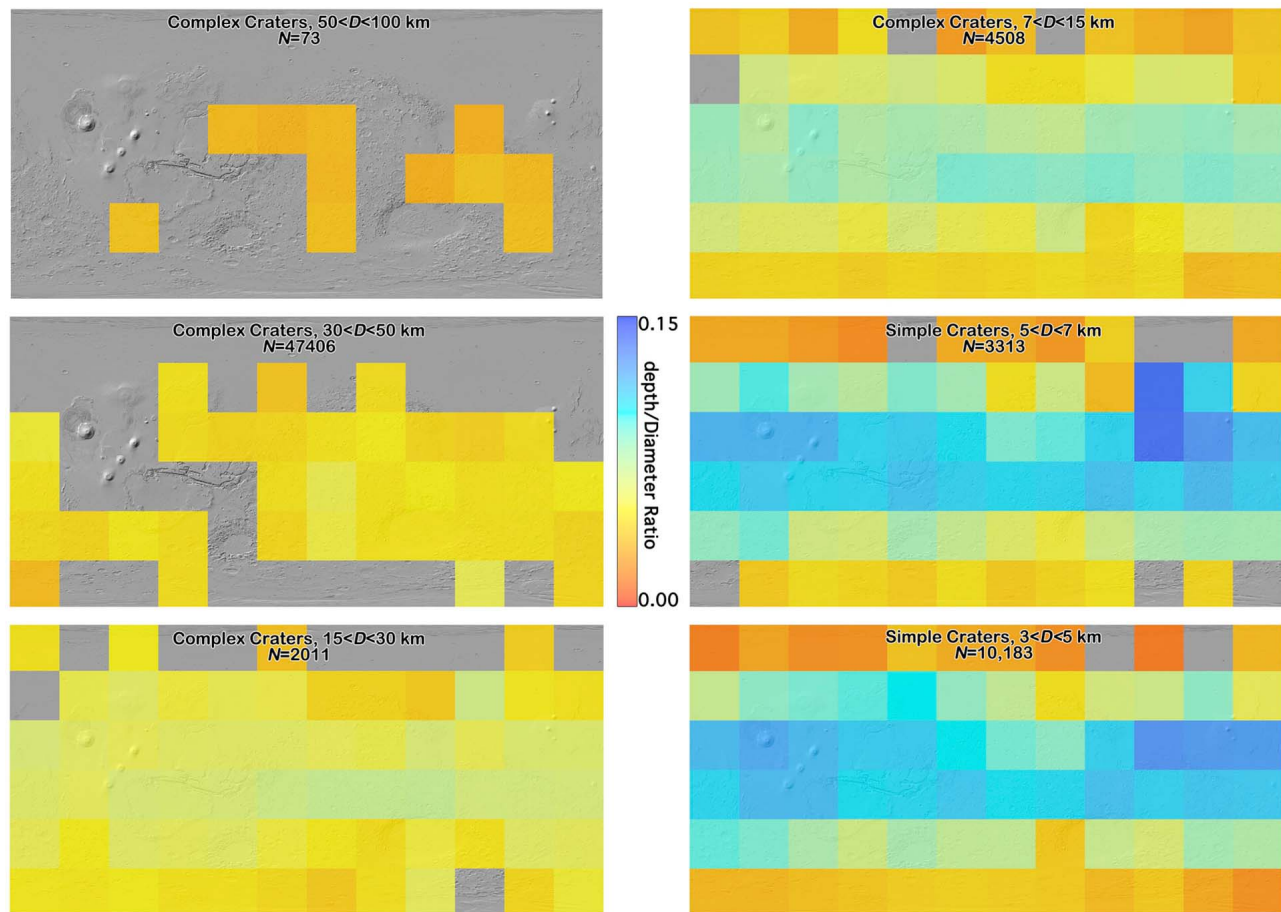


**Figure 10.** Six panels showing binned fresh (degradation states 3 and 4) crater depth/Diameter ratios across Mars in  $30^\circ \times 30^\circ$  bins; bins with  $N < 5$  craters were removed. Four panels show complex craters and two are simple.

excavating to a more uniform basal layer across the planet, and subsequent modification occurs more uniformly and is less controlled by regional upper crust strength. The pattern at smaller diameters of shallower craters toward the poles is likely explained by a near-surface cryosphere [Boynnton *et al.*, 2002] that is weaker and cannot support a deep crater, relaxing to a shallower depth during the crater modification stage and subsequent geologic time. This implies that the crust overlying the major impact basins Chryse, Isidis, and Utopia, is stronger than the average Martian surface today, supporting the deeper crater cavities. Expanding upon the argument from Boyce *et al.* [2006], this shows that the local crust is stronger by at least a factor of  $2\times$  than most other surfaces on Mars. Mineralogical mapping in future work may help characterize the rock, as there are suggestions of regional olivine-rich volcanic units in southern Isidis that may play a role in this [Hamilton *et al.*, 2003; Hoefen *et al.*, 2003]. Alternatively, the similarity with deeper craters on volcanic terrain and the gravitational load in the regions suggest these basins may be buried by volcanic material, and that could be stronger than the average Martian crust to  $\sim 1$  km depths [e.g., Searls and Phillips, 2007]. A separate hypothesis is that the terrain may be particularly fine-grained in some areas of these basins, and work suggests [e.g., Soderblom *et al.*, 1973, 1974; Schultz and Lutz, 1988] that

fine-grained fill materials can produce anomalously deeper craters and this material is found in at least some of these regions.

## 5.2. The Depth-Diameter Relationship for Mars

### 5.2.1. Variation With Latitude and Terrain Type

[37] As is readily apparent from Figure 9, except for craters  $D \gtrsim 30$  km there is no uniform, global depth/Diameter ratio even for a small diameter range that can be quoted for the planet because of a significant shallowing near the poles. This must be taken into account when considering a relationship “for Mars” and when using it to determine different properties at an automated level, such as its role in classifying crater preservation state. Besides being important from a physical standpoint and understanding the near-surface crust, it is necessary to have an a priori estimate for how deep a crater likely was when it formed for purposes of estimating erosion and infilling. For example, if one were to use a global estimate for a  $D = 5$  km simple crater ( $d = 0.8$  km) and found it to be filled with lava with 0.2 km deep cavity remaining, then one would assume 0.6 km of burial. But, if this crater was poleward of  $\sim 40^\circ$ , the actual  $d/D$  relationship yields a fresh-looking crater depth of  $d \approx 0.3$  km, so there is only 0.1 km of infill.

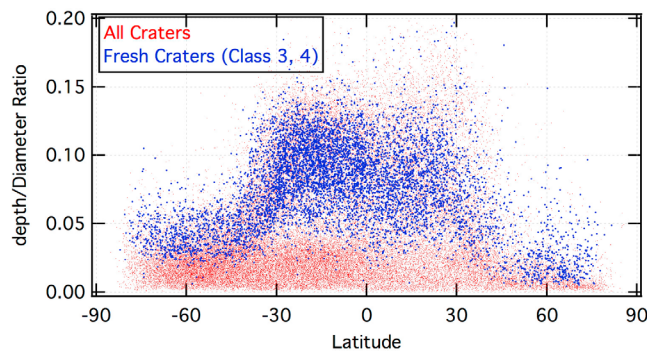


**Figure 11.** Scatterplot showing all craters with only fresh craters (preservation states 3 and 4) over-plotted. Red dots represent all craters and blue symbols are fresh craters.

[38] In the subsections following 5.2.2, craters were separated into seven different regions: First, a global average was done as has been worked on for several decades for comparison purposes. Next, two latitude ranges were analyzed based upon Figure 9 and section 5.2.2 – poleward of  $\pm 40^\circ$  and equatorward of  $\pm 40^\circ$ . Finally, four terrain types were analyzed based on geologic maps by *Scott and Tanaka* [1986], *Greeley and Guest* [1987], and *Tanaka and Scott* [1987].

### 5.2.2. Bimodal Nature

[39] *Stepinski et al.* [2009] clearly showed  $d/D$  are bimodal for craters equatorward of  $\sim \pm 40^\circ$ , the deep craters being “severely depleted southward of  $\sim 38^\circ\text{S}$ .” Their work was among the first to study this in a broad, systematic way, though they used a subset of 2444 craters to do so. Previous research by *Mouginis-Mark and Hayashi* [1993] used 109 fresh craters  $20\text{--}40^\circ\text{S}$  and found a general shallowing trend farther south, but their lack of large numbers of craters limited the spatial analysis and robustness of their work. *Mouginis-Mark and Hayashi* [1993] attributed this to a cryosphere, and *Stepinski et al.* [2009] identified this as a possible contributor, as well. *Stepinski et al.* [2009] also raise the possibility of surficial mantling deposits as suggested by *Soderblom et al.* [1973, 1974]. *Kreslavsky and Head* [2003] propose summertime melting of ground ice at  $\pm 40\text{--}50^\circ$  latitude which could also be a cause. *Boyce and Garbeil* [2007] used a test population of 6047 craters throughout the planet and concluded with a different interpretation: They suggest there is a gap in crater ages separated by the Late Noachian/Early Hesperian boundary that was the result of “abrupt onset and cessation of an episode of terrain degradation” as suggested by *Craddock and Maxwell* [1993]. This would reflect a very rapid  $10\ \mu\text{m}/\text{yr}$  erosion/infill rate (current estimates are  $\sim 1\text{--}10\ \text{nm}/\text{yr}$  [*Golombek et al.*, 2006]). They suggest the contrast with higher latitudes indicate these erosion processes were not active there or other processes erased their effects.

[40] Similar results are found in this database, as illustrated in Figure 11. Simple craters tended to have slightly deeper  $d/D$ , as would be expected from section 5.1; so, they are not plotted separately. In Figure 11, two different data sets are shown – the overall results for all craters as small red dots and craters with a preservation state of 3 and 4 as larger blue dots. This work finds results similar to *Boyce and*

*Garbeil* [2007] and *Stepinski et al.* [2009], but from a larger database, more detail can be gleaned.

[41] First, the same pattern of a gradual  $d/D$  decrease in the deepest craters occurs over the  $\sim 10^\circ$  range of  $\pm 30\text{--}40^\circ$  latitude. However, the north and south hemispheres vary in the magnitude of the difference. In the south, which is where previous studies looked (likely due to the larger crater population in that hemisphere), the  $d/D$  changes from a relatively tight cluster around  $\sim 0.08\text{--}0.14$  and decreases to  $\sim 0.04$  with outliers that go up to  $\sim 0.10$ . In the northern hemisphere, there is significantly more spread with  $d/D$  ranging from  $\sim 0.08$  up to  $\sim 0.20$ . In the higher northern latitudes, there is a shift where a large number of craters are concentrated at shallow  $\sim 0.02$  ratios but with a nontrivial number of craters as deep as  $\sim 0.05\text{--}0.10$  at high northern latitudes. Most of this is reflected well in the “all craters” population in Figure 11.

[42] Another observation is that the pattern is mirrored in the fresh craters, but this begs the question of what is considered “fresh” at  $\pm \sim 60^\circ$  latitudes. The relatively large fraction (up to  $\sim 1/3$ ) of craters in higher northern latitudes that were classified as “fresh” [see *Robbins and Hynek*, 2012] implies that many of these may not be as pristine as they appear. Numerous researchers [e.g., *Schultz and Lutz*, 1988; *Tanaka*, 2000, *Head et al.*, 2003] have discussed the true polar wander of Mars over  $10^5\text{--}10^6$ -year timescales which are much shorter than the formation time of these craters [*Ivanov*, 2001]. While they were interpreted as “fresh” given the morphologic and morphometric criteria discussed in *Robbins and Hynek* [2012], they have likely experienced some amount of infilling.

[43] An interpretation is the northern/southern hemisphere discrepancy can be partially explained by the presence of large impact basins and volcanic complexes in the northern hemisphere that contain the deepest craters on the planet (see section 5.1). However, this is not adequate for the higher northern latitude discrepancy. A possible explanation is that the crust in the southern hemisphere may be more cohesive and stronger, allowing it to support deeper crater cavities, though this seems to run contrary to the “softened” terrain found in higher southern latitudes [e.g., *Jankowski and Squires*, 1992]. In the north, the ice table may be both thicker and closer to the surface – indeed, *Phoenix* at  $68.22^\circ\text{N}$  found ice just a few centimeters from the surface [*Smith et al.*, 2009]. The enhanced relaxation cannot support deep craters, so even otherwise morphologically fresh craters are still comparatively shallow. Another possible contributing factor could be there is more diverse terrain in the higher southern latitudes than in the north. In the north, the northern part of Tharsis and Utopia are present, but otherwise the terrain is predominantly the low northern plains and polar cap. The high southern latitudes contain major volcanoes, the southern half of the comparatively fresh Hellas and Argyre basins, southern highland terrain, and the residual polar cap. While these are offered as likely contributing factors, this should be an area of future investigation.

### 5.2.3. Deepest Craters Method

[44] Arguably, measuring the deepest, freshest craters is likely to produce the best estimate of the original, pristine, crater depth-to-diameter ratio. This method has been utilized in the past several times, notably by *Garvin et al.* [2003] and *Boyce and Garbeil* [2007]. The former used the deepest 25%

**Table 2.** Crater Depth/Diameter Ratios on Mars Over Different Terrains<sup>a</sup>

	Deepest Craters	Fresh Craters	All Craters
Global			
Smp ( $N = 37,091$ )	$d = 0.179D^{1.012}$	$d = 0.097D^{1.061}$	$d = 0.047D^{1.284}$
Cpx ( $N = 32,021$ )	$d = 0.286D^{0.582}$	$d = 0.250D^{0.527}$	$d = 0.107D^{0.559}$
$-40^\circ$ to $+40^\circ$			
Smp ( $N = 24,875$ )	$d = 0.175D^{1.022}$	$d = 0.084D^{1.245}$	$d = 0.078D^{1.106}$
Cpx ( $N = 22,290$ )	$d = 0.280D^{0.570}$	$d = 0.229D^{0.567}$	$d = 0.155D^{0.464}$
$\leq -40^\circ, \geq +40^\circ$			
Smp ( $N = 12,210$ ):	$d = 0.177D^{0.724}$	$d = 0.083D^{1.073}$	$d = 0.014D^{1.465}$
Cpx ( $N = 9742$ )	$d = 0.244D^{0.579}$	$d = 0.174D^{0.629}$	$d = 0.032D^{0.881}$
Northern Plains			
Smp ( $N = 3693$ )	$d = 0.165D^{1.094}$	$d = 0.073D^{1.311}$	$d = 0.011D^{1.992}$
Cpx ( $N = 1308$ )	$d = 0.479D^{0.359}$	$d = 0.274D^{0.502}$	$d = 0.227D^{0.158}$
Volcanic Terrain			
Smp ( $N = 2471$ )	$d = 0.212D^{0.886}$	$d = 0.182D^{0.718}$	$d = 0.091D^{1.010}$
Cpx ( $N = 1008$ )	$d = 0.291D^{0.526}$	$d = 0.240D^{0.539}$	$d = 0.209D^{0.451}$
Southern Highlands			
Smp ( $N = 23,087$ )	$d = 0.235D^{0.777}$	$d = 0.154D^{0.821}$	$d = 0.051D^{1.261}$
Cpx ( $N = 23,850$ )	$d = 0.303D^{0.571}$	$d = 0.231D^{0.556}$	$d = 0.112D^{0.541}$
Polar Terrain			
Smp ( $N = 727$ )	-	-	$d = 0.0028D^{1.843}$
Cpx ( $N = 202$ )	-	-	$d = 0.014D^{1.161}$

<sup>a</sup>This table shows the simple (top line) and complex (bottom line) depth/Diameter relationship when they are divided into a variety of terrain types. The number  $N$  of craters in this table is the number used in the “All Craters” analysis.

of their simple craters from which they estimated a  $d = 0.21D^{0.81}$  relationship from 469 craters for  $D \leq 6$  km, and  $d = 0.36D^{0.49}$  for complex craters  $D > 6$  km. The latter examined craters  $12 \leq D \leq 49$  km and found a relationship of  $d = 0.315D^{0.52}$ .

[45] The methodology of *Boyce and Garbeil* [2007] is what was used here: They separated craters into diameter size bins and iteratively used the single deepest, average of the two deepest, average of the three deepest, etc. craters in each bin through which to fit a power law. They found the slope of the power law was a constant  $0.52 \pm 0.004$  despite increasing the number of craters, while the amplitude of the power law fit changed from 0.363 to 0.356 to 0.333, decreasing with increasing numbers of craters. This was expected and helped to confirm they were sampling the results of the underlying physical process rather than secondary effects, and it produced a more robust result. The value quoted above is for the five deepest craters.

[46] Repeating their example, craters from this database were binned in multiplicative  $2^{1/8}D$  bins. The deepest two craters were averaged together and a power law fit, then the deepest 3, 4, 5, 10, 15, 20, and 25 per bin. For complex craters  $6 < D < 90$  km, the exponent reached a constant level for  $\geq 3$  craters per bin with a mean  $0.582 \pm 0.008$ . While this is slightly greater than their value, it is still fairly close and can be explained because of the use of a larger data set and diameter range. Also similar to their results, the amplitude started large at 0.360 and proceeded to decrease linearly when including 4 or more craters. While a smaller amplitude is reported here than in *Boyce and Garbeil* [2007], this can be explained in that their definition of crater depth was average rim height to the deepest pixel on the floor; the definition used in this database was average rim height and the average of at least 3 floor pixels.

[47] The analysis for simple craters was not as straightforward. The exponent on the fit varied significantly until at least four craters were included, at which point the mean was

$1.012 \pm 0.020$ . This is steeper than *Garvin et al.* [2003], but the robustness of this exponent in other analyses in this work indicates it is likely not anomalous. The amplitude of the fit decreased dramatically from a maximum of 0.271 to an average of  $0.179 \pm 0.001$  for the 10–25 deepest crater fits.

[48] Based on this work, the averages are what will be quoted as the “final” values for the global depth/Diameter relationship on Mars for these craters and are reported in Table 2. The amplitude from the 4 deepest craters fit for complex craters is used because that was the onset of an observed linear decline. When exploring this further, the craters were separated into regions – northern plains, southern highlands, polar, and volcanic – and separated by latitude – equatorward of  $\pm 40^\circ$ , and poleward of  $\pm 40^\circ$ . The regressions were again run, and the results are in Table 2.

[49] Both simple and complex craters poleward of  $\pm 40^\circ$  latitude had no convergence upon a single value for either the exponent or amplitude of the fit for simple and for complex craters. This may be due to relatively small number statistics, but there were still several thousand craters being analyzed and this is an unsatisfying and unlikely reason. Since it is for  $N = 10$  craters that a predictable pattern emerged, it is those values quoted in Table 2 and used in determining crater preservation state for this latitude range [see *Robbins and Hynes*, 2012]. A similar pattern was present for  $N \geq 5$  craters for the complex craters, thus, it is the  $N = 5$  regressions quoted in Table 2 and used to determine crater preservation state. Of interest, the complex slope is very similar to that for the globe, but the slope for simple craters is significantly shallower. This is likely due to two main reasons. First, as identified in *Boyce et al.* [2006] and discussed in section 5.1, the very deepest and largest simple craters are in Chryse, Utopia, and Isidis, generally south of  $40^\circ N$  latitude; while these will be included in the global analysis, their absence here will decrease the amplitude of the largest few diameter bins and hence decrease the exponent. Related, the second likely contributing factor is that the

crustal strength is significantly less, and the inability to support deeper cavities will likely scale with crater diameter, also decreasing this exponent.

[50] While the relationship poleward of  $\pm 40^\circ$  was subject to significant differences, perhaps unsurprisingly the relationship equatorward of  $\pm 40^\circ$  was very similar. This is easily explained by the deepest craters being in this region of the planet and so an algorithm designed to capture the deepest ones would pick up on these in a global distribution. Overall, the results are in good agreement with the global average and are within the quoted ranges.

[51] Analysis by terrain type for the deepest craters method yielded higher amplitudes for the complex crater  $d/D$  relationship for all three analyzable terrains (polar craters numbered too few to be analyzed with this method). The difference was greatest in the northern plains where the amplitude was fully 67% greater than the global function. However, the exponent was significantly shallower, only 62% of that for the global relationship. This would indicate that smaller craters start out deeper in the northern plains but then do not increase in depth as rapidly. Similarly, the exponent on the simple crater function for the volcanic terrain and southern highlands was shallower while the amplitude was just slightly higher, indicating a similar trend to complex craters in the northern plains.

#### 5.2.4. Fresh Craters Method

[52] Recent work to define the  $d/D$  relationship for Mars [e.g., *Garvin et al.*, 2003; *Stewart and Valiant*, 2006] has generally relied upon identifying and measuring the depth and diameter values of morphologically fresh/pristine craters. The *Garvin et al.* [2003] results are described above and agree generally well with the deepest crater method. *Stewart and Valiant* [2006] limited their analysis to five regions on Mars and examined relatively few craters in each: Acidalia Planitia ( $N = 29$ ), Utopia Planitia ( $N = 53$ ), Isidis Planitia ( $N = 24$ ), Lunae Planum ( $N = 48$ ), and Solis Planum ( $N = 33$ ). Utopia and Isidis were identified previously in this work, *Boyce et al.* [2006], and *Stepinski et al.* [2009] as having deeper craters than the average terrain, and they found larger  $d/D$  when just looking in those regions ( $d = 0.404D^{0.41}$  for Utopia and  $d = 0.351D^{0.41}$  in Isidis). Acidalia is north of the Chryse impact basin and is around the region identified above as also having deeper than average craters, and they identified a relatively deep crater relationship there, as well, of  $d = 0.384D^{0.38}$ . Interestingly, the slopes in all of these relationships are shallower than identified by the work from this crater database, indicating that they found, by comparison, either smaller craters to be deeper or larger craters to be shallower. Another possible explanation is that there may be relatively large uncertainties due to the comparatively small number of craters in their study.

[53] The analysis in this section mimics this approach and only uses craters that are classified with a preservation state of “4” (fresh). This process is slightly incestuous because one of the four parameters in crater preservation state is the crater depth relative to the established  $d/D$  relationship. To minimize how recursive this process is, the deepest crater  $d/D$  was used to define that part of crater preservation state such that this fresh crater method could be relatively independent. Overall, 2704 craters  $D \geq 5$  km were identified as “fresh” in this database (an additional 3603 craters  $3 \leq D < 5$  km were fresh, but they were not used in this

analysis due to larger uncertainties). Of those, 934 were classified as simple (831 were equatorial of  $\pm 40^\circ$  and 103 poleward), and 1060 were complex (976 were equatorial of  $\pm 40^\circ$  and 84 were poleward).

[54] As an overall global average, the slope of the fresh simple and complex craters was similar to the deepest crater method, varying at the few-percent level and likely within the noise. The amplitude of the fit is expectedly smaller, though the difference is roughly a factor of  $2\times$  for simple craters but  $\sim 15\%$  for the complex craters. This is easily explained in that the fresh craters method is sampling an ensemble of terrains (the whole planet) and that the deepest crater method is simply picking the deepest ones which have been shown to be terrain-dependent. The relative lack of a difference at the larger, complex crater diameters can be interpreted as these craters are less dependent upon terrain type than smaller craters and therefore there are fewer deepest craters that then get averaged out.

[55] Regressions were again run for the subregions, and the results are shown in Table 2. Overall, the separation by latitude range is similar to the trend found for the deepest craters, though small numbers toward the poles ( $N = 103$  for simple and  $N = 84$  for complex) may limit the robustness of the fits. Analysis of the polar terrain craters could not be done because the numbers were too small. Overall, the terrain separation did not yield significantly different results than the global analysis except in three values. First, the exponent in the simple crater fit for the northern plains was substantially steeper than both the global average and equatorial range. Second, the amplitude for the simple craters in volcanic terrain was twice that of the global average and the latitude separations, indicating that simple craters start substantially steeper in volcanic terrain, but the exponent was smaller, indicating that as they increase in diameter, the depth does not grow correspondingly as large as for the global average.

#### 5.2.5. Average Across Crater Depths and Preservation States

[56] An additional method that may have dubious intrinsic physical meaning is that of taking an overall average of depths of craters for a given diameter. This was done in *Stepinski et al.* [2009] to define  $d = 0.025D^{1.6}$  for simple craters  $D < 7$  km, and  $d = 0.22D^{0.47}$  for complex craters  $D \geq 7$  km based on a combined total of 3666 craters. Earlier, *Garvin et al.* [2003] produced overall average results for simple craters  $D \leq 6$  km of  $d = 0.21D^{0.80}$  from 2263 craters. This is only slightly different from their results for the deepest craters, and it is significantly different from the *Stepinski et al.* [2009] function.

[57] Fitting was done in the same manner as the previous sections, and results are reported in Table 2. In this case, all craters were included in these numbers. Globally, the complex crater function was similar in slope to the overall average, though it was slightly shallower, and the amplitude was 37%. This indicates that as a whole, Mars' crater population has been infilled/modified relatively evenly across diameter ranges, though there may be slightly more infilling at larger sizes. This is interpreted as larger craters are generally older and so would be more infilled on average than a broader age range at smaller diameters. The simple crater population is significantly different, for it has an amplitude of 26% the deepest craters but an exponent 27% greater.

Borrowing from the above interpretation, this indicates that more small simple craters are significantly infilled than larger ones. While this may be the case, it could also be an artifact of the MOLA data used in this analysis as discussed in *Robbins and Hynes* [2012] and the beginning of this section. Further work examining each crater with MOLA shot data and/or comparison with higher resolution DTMs are necessary to resolve whether the latter issue is a significant factor. Both of these are significantly different from *Stepinski et al.*'s [2009] results.

[58] Division of the craters along the  $\pm 40^\circ$  latitude lines resulted in somewhat different results to those found in section 5.2.3 with the deepest craters. Poleward of  $\pm 40^\circ$ , the amplitude of the fits decreased by a factor of  $\sim 3\times$ , while the amplitude of the fits for craters equatorward of  $\pm 40^\circ$  increased by a factor of  $\sim 1.5\times$ . The equatorial craters' exponents dropped by  $\sim 20\%$  while the polar simple craters rose by 14% and complex by 58%. This was the steepest complex crater relationship found in this work except for the polar terrain separation. Interpretation of these results for amplitude is straight-forward and discussed above, for polar craters are shallower because of a weaker crust likely due to a cryosphere. The hypothesis discussed above that the anomalously large exponent for simple craters may be due to MOLA artifacts should be less significant near the poles because of higher point density due to the *Mars Global Surveyor* orbit; thus, these results should be *more* robust than their equatorial counterparts, but the slope is greater. If this is a real phenomenon, this would indicate the former interpretation for the global results is more likely, that smaller craters are more infilled than larger ones, which would seem to belie a normal sequence of events: larger craters preferentially form earlier in the history of a surface while many more smaller craters form later. If one can assume an even infilling/erosion rate, the  $d/D$  slope should remain fairly steady while the amplitude decreases. More work on this issue should be done to unravel this result.

[59] The all-crater average when craters were separated by terrain yielded a few interesting results. First, the polar terrain craters were significantly shallower than the global average, but the power law exponents were significantly steeper by 43% and 107% for simple and complex curves. This could be explained by the proposal in section 5.1: Smaller craters ( $3 \leq D < 7$  km) will be effected by the terrain much more than larger craters. Thus, the polar terrain will cause a significantly shallower crater, but as craters get larger the terrain dominance lessens and normal scaling dominates. An alternative explanation (P. Schultz, personal communication, 2012) is that smaller craters may be more efficient at trapping deposits of ice and other material from a moving ice cap, whereas larger craters could be more easily exhumed due to their boundary conditions.

[60] Otherwise anomalous were the craters on volcanic terrain with amplitudes a factor of  $2\times$  greater than the global average. However, this can be fairly easily explained by fresh craters dominating Martian volcanic terrain (64% are preservation states 3 or 4) and so more modified, shallow craters do not lower the average.

### 5.3. Synthesis of the Depth/Diameter Relationship

[61] Crater depth/Diameter relationships are an important tool to understanding how craters form and then how craters

differ from what is expected. Investigation into this relationship was done in three main ways – deepest craters, fresh craters, and all craters – and for the entire globe, different latitude bands, and specific terrain types. Overall, the results are reasonably consistent with most previous work in this area [e.g., *Garvin et al.*, 2000, 2003; *Stewart and Valiant*, 2006; *Boyce and Garbeil*, 2007] though varied from the automated analysis of *Stepinski et al.* [2009].

[62] Within the nineteen different method-region combinations for both simple and complex craters, the results were generally self-consistent. Variations were expected due to the particular analysis conducted. For example, the deepest craters method consistently yielded the deepest  $d/D$  relationship while the all-crater averages were always the shallowest. The exponent slopes were also generally consistent among each other, though a few outliers did exist as explored in the previous subsections. Overall, it is reassuring that the different methods yielded similar results with most differences easily explained. This is the first work to examine these relationships through multiple methods and compare them.

[63] Application of this analysis to future research should probably be limited to using the deepest craters method results when separated by terrain type. If a crater is emplaced in a terrain that was not covered by the four major ones analyzed here, then researchers should use the latitude bands. Using the global average will result in underestimating original crater depth in some cases such as on volcanic terrain, or overestimating original depth in locations such as near the poles.

## 6. The Simple/Complex Morphology Transition

[64] Simple craters are small with concave floors while complex craters are large and have a variety of interior morphologies such as wall terraces, central peaks, and flat floors. Fundamentally, the transition diameter between simple and complex craters has been observed to be a function of the surface gravity of the target object [e.g., *Baldwin*, 1949; *Quaide et al.*, 1965; *Malin and Dzurisin*, 1977; *Pike*, 1977, 1980a]. However, it is also at least in part controlled by target material strength [e.g., *Pike*, 1980b, 1988]. Determining the diameter at which an impact crater will transition from simple to complex morphology can inform studies of the target, its properties, and the role of gravitational collapse and elastic rebound. These are the main mechanisms during crater formation's modification phase that produce complex morphologies. While the diameter of this transition is necessarily a range because different morphologies will begin to form at different diameters, the diameter of this transition was found to be roughly 6 km for Mars with no significant terrain dependence [*Pike*, 1988]. This value has been argued about over the years with each new data set of craters, and in that tradition this database was mined to determine if *Pike's* [1988] synthesis requires revision.

[65] In that spirit, this section examines four different types of simple-to-complex transitions – basic floor morphology, onset of central peaks and terraces, and depth/Diameter transitions – for the globe, latitude ranges, and terrain type. Any deviations from the canonical value have implications for the surface material and can be used as a tracer for that.

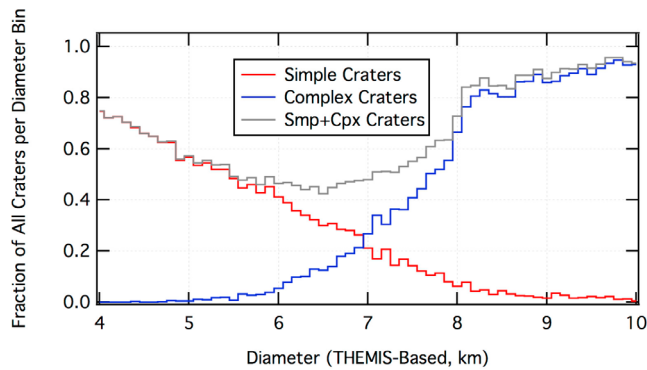


**Figure 12.** Three histograms were created as a function of diameter: All craters, simple craters, and complex craters. The simple and complex crater histograms were divided by the histogram for all craters and are plotted here, their sum shown in gray. The deficit relative to 100% of all craters being classified between  $\sim 5$ –8 km is due to the conservative classification to avoid classifying infilled simple craters as flat-floored pristine complex craters and vice versa.

### 6.1. Based on Floor Shape

[66] A crater is considered to be within the basic complex type when it displays a flat floor morphology that is not due to post-formation infilling. Additional features are often characteristic of complex craters, but these are addressed in subsequent sections. Toward the goal of discerning the average diameter transition from simple to basic complex morphology, all craters in the database were classified from the available data - if possible - into these basic types. Craters in the  $\sim 4$ –8 km-diameter range were not classified if it was not clear if they were either fresh-appearing complex flat-floored craters or infilled (modified) simple craters [see *Robbins and Hynes, 2012*]. It should be noted that simple craters were observed to be as large as  $D \sim 13$ –14 km, but these were outliers and well above the average transition diameter calculated below.

[67] Three histograms were created to quantify this: all craters, all simple craters, and all complex craters. The simple and complex crater histograms were then divided by the overall database histogram, and these are displayed in Figure 12; the sum of the two is also shown. The simple-complex transition diameter is where the fraction of complex craters is greater than simple craters, and it is 6.9 km (Figure 12). This diameter proved to be robust when separated into the two latitude ranges with the equatorial transition at 7.0 km and polar at 6.9 km. Examining craters at higher latitudes, however, yields interesting results: Poleward of  $\pm 60^\circ$ , the transition occurs at 7.7 km, and at  $> \pm 70^\circ$ , it rises to 8.0 km (this is robust as there are still  $N > 1000$  craters). Separating these by northern and southern hemispheres yields a transition at 8.1 km for  $< -70^\circ\text{N}$ , and those  $> +70^\circ\text{N}$  have a transition  $\sim 8.4$  km. A similar effect was found when separating by terrain type as in section 5.2: Polar terrain craters had a transition of  $\sim 7.9$  km while the other three (northern plains, southern highlands, and volcanic) were  $\sim 7.0$  km. This is similar to findings by *Garvin et al. [2000]*.

[68] The dependence upon latitude and terrain has not been quantified before. As discussed, the transition is a

consequence of collapse under gravity due to surpassing the strength of the target. (Impactor velocity will also play a role in this transition [*Pike, 1988; Schultz, 1988*], discussed in greater detail in section 6.4.) This runs contrary to what one would expect for the Martian crust for, as graphically illustrated in section 5, the higher latitudes of the planet are likely dominated by a near-surface cryosphere [*Boynton et al., 2002*] and the cryosphere at northern latitudes is probably closer to the surface (section 5.2.2). From this, one would expect an impact into an ice-solidified crust would vaporize volatiles and weaken the crust, permitting gravitational collapse to a complex crater at smaller diameters rather than strengthening it for transitions at larger diameters. One possible explanation is that water in the surface causes it to act more fluid during the modification phase of crater formation, resulting in material gently sloping down the crater walls, shallowing the bowl, but maintaining the bowl shape overall. Another explanation is that infilling or general blanketing as a consequence of obliquity cycling could account for some or all of this effect.

### 6.2. Simple-Complex Transition Based on Other Complex Crater Morphologies

[69] Although *Pike [1980b, 1988]* examined several morphologies (flat floor (addressed above), central peak, scalloped rim, terraced wall, ballistic ejecta, flow ejecta), in this analysis the morphologies are limited to two additional ones – central peaks and terraced walls. Central peaks form by rebound of the crust during crater formation [e.g., *Wood, 1973; Roddy, 1976*]. Terraces are a collapse feature from the walls during crater formation; basic wall collapse, such as talus, was not considered here. While these are fundamentally different processes, and they will manifest at different crater sizes, they are each a good morphologic indicator of failure of the crust to support a simple bowl and hence display a complex crater. Craters were binned similarly as in the basic morphology, discussed above. An average was taken at the diameter where the fraction of the craters that contained the feature was stable. Then, the diameter at which 50% of the average was reached was considered the transition diameter.

[70] Central peaks were present in an average of 6.3% for craters of all preservation states with diameters  $D \geq 15$  km. 50% of this was reached at  $D = 5.6$  km. The smallest crater with a central peak was  $\sim 2$  km, but it did not reach 5% of the steady state 6.3% level until  $D \geq 3.3$  km. The same analysis on equatorial craters shows a smaller diameter transition  $D = 4.8$  km, while the  $> \pm 40^\circ$  latitude range yielded a larger diameter of 11.3 km. Similar results were found on volcanic and southern highlands terrain while there were not enough craters for an analysis on polar deposits. The northern plains were significantly different with a transition to central peaks at  $D = 8.4$  km.

[71] Terrace morphology did not reach a steady state until  $D \approx 15$  km, and this was at a level of 21%. 50% of this was reached at  $D = 8.3$  km. The smallest crater with wall terraces was  $\sim 3$  km, but it did not reach 5% of steady state until  $D \geq 4.5$  km. The same analysis on equatorial craters shows a slightly smaller diameter transition of  $D = 7.5$  km, while the  $> \pm 40^\circ$  latitude range yielded a significantly larger transition diameter of 16.9 km. Terrain-dependent results were similar to the global average except for polar where

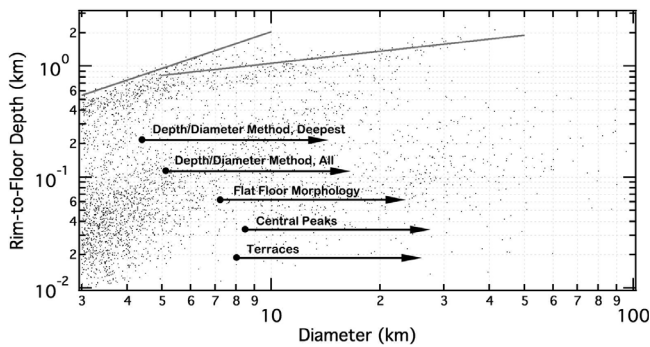


**Figure 13.** Simplified diagram illustrating the diameter at which the simple-complex transitions are observed for the northern plains. Dots are craters, and the two nearly crossing lines are the best fits for simple and complex deep craters. Arrows indicate the transition diameter from simple to complex for each of the labeled characteristics examined (vertical offset is arbitrary).

again small numbers made this analysis difficult; the smallest diameter crater with visible terraces on polar terrain was 10 km.

[72] These values are in rough agreement with *Pike* [1980b] who found transition diameter from central peaks and terraces to be in the 6–8 km-diameter range with the prevalence of wall terraces at larger diameters than central peaks (the worker found a difference of a factor of  $2\times$ , though this work and methodology shows it to be  $1.5\times$ ). The latitude range-dependent trend observed here supports the idea from flat floor morphology that it is more likely this is a real feature of the craters rather than an error in classification.

[73] Issues with erosion of these more complex features are likely significant, for one would expect the vast majority of larger complex craters form with terraced walls and likely central peak features from basic cratering physics [*Melosh*, 1989]. For example, when only examining fresh craters, terraces were identified in  $>90\%$  of craters  $D \geq 20$  km, and central peaks were present in 55% of  $8 < D < 13$  km craters and  $>90\%$  of  $D > 14$  km craters. However, we expect that our ability to visually identify the presence of these features will be fairly uniform in the  $\sim 10$ –20 km-diameter range despite erosion, and tests of examining hundreds of craters classified as “pristine” showed comparable results.

### 6.3. Simple-Complex Transition Based on Depth/Diameter

[74] A more common method of determining transition diameter is on a crater depth versus diameter plot (e.g., Figure 13). On these, simple craters have a relatively steep slope compared with complex craters, and there will be a slope discontinuity where they intersect. Some overlap is present due to target, impactor, and other variances, but in general this occurs over a narrow diameter range. When fitting the slopes to a power law function (section 5.2), there is an exact diameter at which the slopes intersect. This diameter is what is used and reported here.

[75] Globally, for the deepest craters method, the transition diameter is 3.0 km. The fresh crater method puts the transition at 5.9 km, while the all-crater average is 3.1 km.

Transitioning to the equatorial latitude band, the diameter goes down slightly for all cases - following the pattern in the previous two sections - to 2.8 km, 4.4 km, and 2.9 km. The higher latitudes saw mixed results with a spurious 9.2 km result for the deepest craters method due likely to small numbers, 5.3 km for the fresh method, and 4.2 km for the global average. These values are also considered to be similar and non-significant in terms of differences except in the higher latitudes (see below). Overall, these are nearly all smaller than the simple-to-complex transition diameter than when based upon morphology alone. This phenomenon was observed in previous work by *Pike* [1988] not only on Mars, but also on Earth, Mercury, and the Moon. A figure similar to his Figure 11 is shown as Figure 13, illustrating this point as well as showing the general diversity of the onset of these morphologic and morphometric characteristics.

### 6.4. Synthesis of the Simple/Complex Morphology Transition

[76] Overall, this is the first work to utilize a modern global crater database to examine the simple-to-complex morphology transition on Mars. It does so with respect to multiple morphologic and morphometric indicators and a latitude and terrain dependence. The results of this analysis of independent morphologic and morphometric transitions are summarized in Figure 14 and Table 3. Only the transition diameters for the deepest craters’  $d/D$  relationship are used to calculate the arithmetic and geometric means (except for polar terrain). These means are very close to each other, and the standard arithmetic would normally be used, but *Pike* [1988] used geometric so that is included as a comparison. The means for the global distribution are 6.0 km average and 5.6 km geometric; the standard deviation is  $\pm 2.3$  km. *Pike* [1988] calculated  $\sim 6$  km for the transition. The other results are in Table 3.

[77] This work supports *Pike*’s [1980a, 1988] analysis from *Viking* images that found different transition diameters for different simple/complex morphologies, as is indicated by the overlap shown in Figure 15. It is, however, significantly more robust, utilizing thousands of craters across the globe instead of 230 craters. It used a variety of modification states as well as and only fresh craters as a check. The global results fit very well within *Pike*’s [1988] synthesis and lie directly upon the lower dashed line of Figure 15 that indicates similarity with sedimentary rock on Earth. However, caution should be made in the interpretation of this figure, for impactor velocity will play a role in this transition [*Pike*, 1988; *Schultz*, 1988] which can account for the failure of Mars and Mercury to (a) be similar and (b) lie on the Earth-Moon line.

[78] Of particular interest is the latitude and terrain dependence shown. This result was robust in the previous sections: The equatorial range of  $< \pm 40^\circ$  latitude showed slightly smaller diameter transitions while the polar latitude range had craters that transitioned at significantly larger diameters for nearly all morphologic and morphometric indicators (though the ranges do slightly overlap, as shown in Figure 14). The implication is that crust type that dominates in the equatorial band of Mars is less competent and craters will undergo gravitational collapse during the modification phase of formation more readily. Meanwhile, the crust closer to the poles is more competent and less prone to

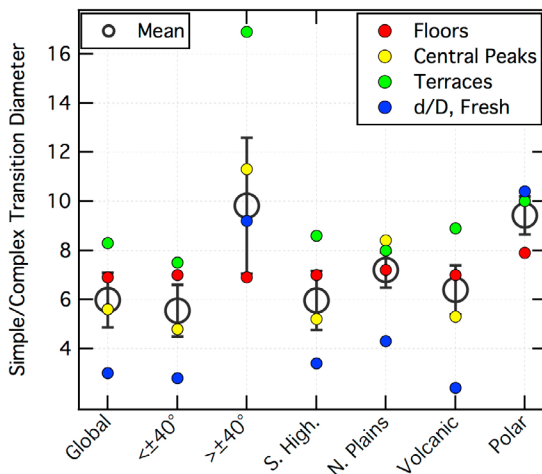


**Figure 14.** Combined results from using different morphologic and morphometric indicators to determine the transition between simple and complex crater morphology on Mars. Solid circles are points showing each result discussed in the text, the key to which is shown by the legend to the upper right. Black open circles are the arithmetic means for all morphologic data and results from the deep crater  $d/D$  method (since that is considered the most robust technique (see sections 5.2 and 5.3)). Error bars are the standard deviation from the means of the three or four values divided by  $\sqrt{N}$ .

this form of collapse. Interestingly, this runs contrary to the basic interpretation of crater depth/Diameter data discussed in section 5. That indicated the crust was weaker near the poles because even morphologically fresh craters were a factor of  $\sim 2\text{--}3\times$  shallower than their equatorial counterparts. An alternative or additional explanation to reconcile these could be that dusty deposits at high latitudes may prohibit slump blocks forming at smaller sizes, causing the transition to complex morphology to be at larger diameters. These disparate relationships are addressed in section 7.

## 7. Discussion and Conclusions

[79] We have explored the basic crater distributions, morphologic distributions, morphologic relationships, and morphometric relationships from a new global crater database of Mars. This database was shown to be statistically robust [Robbins and Hynek, 2012], and we examined many

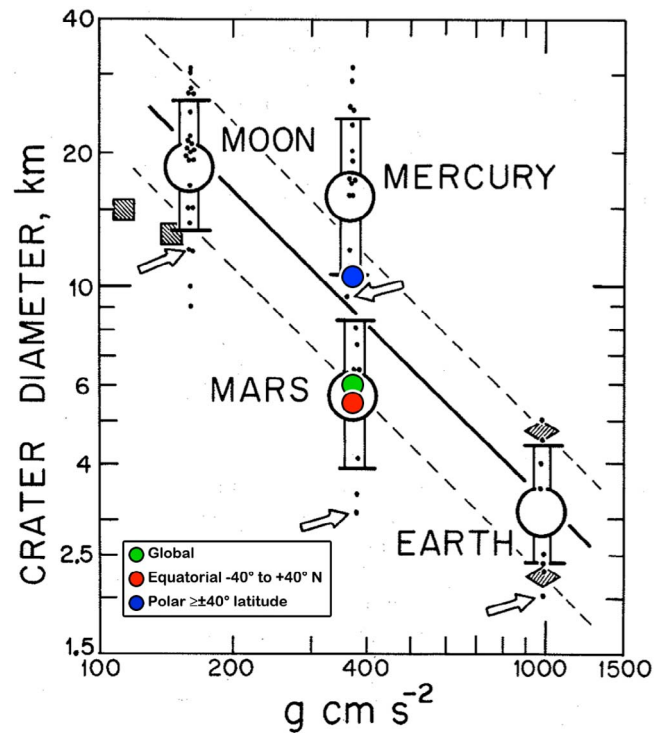


**Figure 15.** Background figure is adapted from Pike [1988], illustrating surface gravity versus onset of complex crater morphology for the large inner solar system bodies (except Venus) and Ganymede and Callisto (squares). Each small black dot is from Pike [1988] and represents a different morphologic indicator of this transition. Arrows point to  $d/D$  results in the original Pike [1988]. Large circles are geometric means and bars are standard deviations. The solid black line is a best fit, while the diamonds are for different targets on Earth and the dashed lines extrapolations of the fit for those targets (lower is for sedimentary rock, upper is igneous). Used with permission, ©1989 The Arizona Board of Regents, University of Arizona Press. Overplotted in color are the results from this work (arithmetic means).

previously observed trends to illustrate and confirm its agreement with previous work. We also expanded the analysis to illustrate and confirm the utility in discerning new trends and relationships as well as to refine some that have been studied for decades.

**Table 3.** Summary of Transitional Diameters for Different Martian Terrains and Derived Through Various Means Discussed in the Text<sup>a</sup>

	Global	$\leq 40^\circ$	$\geq 40^\circ$	Southern Highlands	Northern Plains	Volcanic	Polar
Floors	6.9	7.0	6.9	7.0	7.2	7.0	7.9
Central Peak	5.6	4.8	11.3	5.2	8.4	5.3	-
Terrain	8.3	7.5	16.9	8.6	8.0	8.9	10.0
$d/D$ , Deep	3.0	2.8	9.2	3.4	4.3	2.4	10.4 <sup>b</sup>
Average Mean	6.0	5.5	11.1	6.1	7.0	5.9	9.4
Global Mean	5.6	5.2	10.5	5.7	6.8	5.3	9.4
Standard Deviation	2.3	2.2	4.3	2.2	1.9	2.8	1.3

<sup>a</sup>All units are km.

<sup>b</sup>There were not enough craters to derive a reliable function for the “deepest” crater method for polar terrain craters. The “all-craters” method value is quoted in its stead, and it was used to compute the averages and standard deviation.

[80] In basic crater distribution across the planet, we showed that smaller diameters illuminate significant new work and forms the bulk of the number of craters in this database. The small crater population shows finer age variations across the surface in contrast with 5–50-km-diameter populations, and it also starts to inform studies of secondary crater populations [Robbins and Hynek, 2011a, 2011b].

[81] Our work examining crater interior morphologies (central peaks, summit pits, and central pits) provides validation of our database, updates older results [e.g., Barlow and Bradley, 1990], and extends other modern ongoing work to the southern hemisphere [Barlow, 2010, 2011]. Central peak distribution generally correlates with fresh craters, but there is disagreement at central longitudes in the southern hemisphere. Further efforts in understanding this should be fruitful, as will further exploration into the distribution of Martian central pits and summit pits. The terrain in which these latter features are found supports a model that incorporates volatiles in their formation [e.g., Wood et al., 1978; Croft, 1981; Senft and Stewart, 2008; Alzate and Barlow, 2011], though the specific model is open to interpretation from our cursory analysis. Morphometric analysis may support this and is underway by other researchers [Barlow, 2010, 2011; Alzate and Barlow, 2011].

[82] The distribution of radial ejecta was found to reproduce relative terrain ages reasonably well despite the craters forming after the terrain, illustrating that radial ejecta can be preserved over long periods of geologic time on Mars. Layered ejecta blanket data is abundant within the database, comprising nearly 50% of the data columns [Robbins and Hynek, 2012, Appendix A]. Extensive mining of these data for purposes of better explaining these features and their formation is the subject of future work, but in this paper we showed its general agreement with previous work in the area [e.g., Mouginis-Mark, 1979; Schultz and Gault, 1979; Barlow and Bradley, 1990; Barlow and Perez, 2003; Barlow, 2005] and demonstrated its utility in refining previous distributions and trends.

[83] Our database provides detailed topographic information about craters, and this has resulted in updating some of the empirical morphometric scaling laws as applied to Mars. Overall, we found that Martian craters display rim morphometries that are  $\sim 2\times$  smaller than their lunar counterparts (summarized in Melosh [1989]). This is the case for rim height and surface-to-floor depth each relative to crater diameter, and these hold for both simple and complex crater morphologies.

[84] In further application to morphometric scaling, we examined the fresh-appearing crater depth-to-diameter ratios ( $d/D$ ) as an update to previously identified trends and values, though this was the first analysis to compare three different methods from the same data set for deriving the  $d/D$  relationships on Mars. We illustrated the known global dichotomy of deeper craters in equatorial regions and shallower craters toward the poles, and we expanded upon this to show a previously unobserved secondary effect of a north/south dichotomy. This shows a wider variation of crater depths toward the equator in the north compared with the south, but the opposite was the case at polar latitudes. The high northern latitude craters showed a very tight and shallow distribution of depths compared with the south, likely indicating a nearer surface cryosphere and more uniform terrain.

We reexamined the basic crater  $d/D$  relationship, as well, for both the global average and subregions. Within each, we characterized  $d/D$  for simple and complex craters in terms of the deepest craters, fresh craters, and all craters. Our results for the global average compare well with previous work, and our results within the terrain dependence reflect the dichotomy observed before. These differences are important, and they must be taken into account when using crater depth to estimate erosion, infilling, and other modification processes. Otherwise, there is the chance of interpreting all high-latitude craters as degraded relative to equatorial ones.

[85] These  $d/D$  results for the deepest craters were then placed into the context of one of the other basic crater morphometric scaling laws in a method similar to what has been done in the past [e.g., Pike, 1977, 1980b, 1988]: At what diameter does a crater transition from simple to complex morphology? Three morphologic indicators were examined - basic morphology (bowl versus flat floor), central peaks, and wall terraces - and the intersection of the  $d/D$  fits were our morphometric criterion. We again segregated by terrain as well as examined the global relationship. Our results agree very well with Pike [1988] for the global population, and this lends credibility to the incredible difference observed between latitude bands: We found the simple-complex transition occurs at  $\sim 11$  km at high polar latitudes rather than the  $\sim 6$  km global average (Figure 14).

[86] Taken with the  $d/D$  information for fresh and deep craters, we propose a model where the higher latitude craters will begin to form as they do elsewhere through the contact and excavation stage [Melosh, 1989]. During excavation, the impact energies will melt and vaporize ices in the nearby, surrounding crust (modeling indicates that more than enough ice would melt [see Kraus and Stewart, 2010; Barr and Citron, 2011]). This will weaken the crust where vaporized, and intense ground movements cause the wet crust to flow like mud. During the modification phase, the crust is not strong enough to support the deep cavity characteristic of equatorial simple craters, but the viscous fluid-rich material will relax, decreasing the crater depth but maintaining a bowl shape. A central peak, generally the first complex morphologic indicator, does not form until  $D \approx 11$  km poleward of  $\pm 40^\circ$  and there were only two found in polar terrain. Either the central peak does not form in this suggested water-saturated crust until significantly larger diameters are reached, or it does form but quickly collapses and does not leave behind a visual indicator it existed.

[87] The effect predicts that simple craters are maintained at larger diameters, but they are shallower than equatorial ones. This is more significant in high northern latitudes where there is likely a nearer surface and/or thicker cryosphere [Boynton et al., 2002] enhancing this process. This is supported by the cohesive layered ejecta morphology distribution found in the northern hemisphere where their presence is also more prevalent than in the southern. The concentration of DLE craters in high northern latitudes supports this, for it is likely that at least this type requires a volatile in the subsurface to form based on the type's abundance over SLE on Ganymede [Boyce et al., 2010], though it could also benefit from finer-grained silts, a lithology-dependence [Schultz, 1992].

[88] Overall, this new crater catalog with 384,343 craters  $D \geq 1$  km is comparable to previous ones where they

overlap, and the additional morphologies and morphometries have proven to be an unparalleled asset in studying the surface of Mars. This database freely available for download via the Mars Crater Consortium section of USGS's PIGWAD server ([http://webgis.wr.usgs.gov/pigwad/down/mars\\_crater\\_consortium.htm](http://webgis.wr.usgs.gov/pigwad/down/mars_crater_consortium.htm)). We have also made a web-query site that allows users to download craters and features based on user-selectable fields and options that is available at <http://craters.sjrdesign.net>.

[89] **Acknowledgments.** The authors thank P. H. Schultz and S. C. Werner for thorough and helpful reviews as well as the Editors M. Wieczorek and D. Baratoux. S. J. Robbins thanks his dissertation committee for feedback used to improve this work: F. Bagenal, N. Barlow, B. Hynek, B. Jakosky, and N. Schneider. This work benefited from the assistance of R. Haber, D. McKenzie, D. Russell, and K. Brugman. Support for this work was through NASA NESSF award NNX07AU85H and NASA award NNX10AL65G.

## References

- Alzate, N., and N. G. Barlow (2011), Central pit craters on Ganymede, *Icarus*, 211, 1274–1283, doi:10.1016/j.icarus.2010.10.015.
- Baldwin, R. B. (1949), *The Face of the Moon*, Univ. of Chicago Press, Chicago, Ill.
- Banks, M. E., S. Byrne, K. Galla, A. S. McEwen, V. J. Bray, C. M. Dundas, K. E. Fishbaugh, K. E. Herkenhoff, and B. C. Murray (2010), Crater population and resurfacing of the Martian north polar layered deposits, *J. Geophys. Res.*, 115, E08006, doi:10.1029/2009JE003523.
- Barlow, N. G. (1988), Crater size-frequency distributions and a revised Martian relative chronology, *Icarus*, 75, 285–305, doi:10.1016/0019-1035(88)90006-1.
- Barlow, N. G. (2005), A review of Martian impact crater ejecta structures and their implications for target properties, in *Large Meteorite Impacts III*, edited by T. Kenkmann, F. Hörz, and A. Deutsch, *Spec. Pap. Geol. Soc. Am.*, 384, 433–442.
- Barlow, N. G. (2010), Central pit, central peak, and elliptical craters in the Martian northern hemisphere: New results from the revised Catalog of Large Martian Impact Craters, *Lunar Planet. Sci.*, XLI, Abstract 1065.
- Barlow, N. G. (2011), Constraints on the proposed formation models for Martian central pit craters, *Lunar Planet. Sci.*, XLII, Abstract 1149.
- Barlow, N. G., and T. L. Bradley (1990), Martian impact craters: Correlations of ejecta and interior morphologies with diameter, latitude, and terrain, *Icarus*, 87, 156–179, doi:10.1016/0019-1035(90)90026-6.
- Barlow, N. G., and C. B. Perez (2003), Martian impact crater ejecta morphologies as indicators of the distribution of subsurface volatiles, *J. Geophys. Res.*, 108(E8), 5085, doi:10.1029/2002JE002036.
- Barlow, N. G., J. M. Boyce, F. M. Costard, R. A. Craddock, J. B. Garvin, S. E. H. Sakimoto, R. O. Kuzmin, D. J. Roddy, and L. A. Soderblom (2000), Standardizing the nomenclature of Martian impact crater ejecta morphologies, *J. Geophys. Res.*, 105(E11), 26,733–26,738, doi:10.1029/2000JE001258.
- Barr, A. C., and R. I. Citron (2011), Scaling of melt production in hypervelocity impacts from high-resolution numerical simulations, *Icarus*, 211, 913–916, doi:10.1016/j.icarus.2010.10.022.
- Boyce, J. M., and H. Garbeil (2007), Geometric relationships of pristine Martian complex impact craters, and their implications to Mars geologic history, *Geophys. Res. Lett.*, 34, L16201, doi:10.1029/2007GL029731.
- Boyce, J. M., P. Mouginiis-Mark, H. Garbeil, and L. L. Tornabene (2006), Deep impact craters in the Isidis and southwestern Utopia Planitia regions of Mars: High target material strength as a possible cause, *Geophys. Res. Lett.*, 33, L06202, doi:10.1029/2005GL024462.
- Boyce, J. M., N. G. Barlow, P. Mouginiis-Mark, and S. Stewart (2010), Rampart craters on Ganymede: Their implications for fluidized ejecta emplacement, *Meteorit. Planet. Sci.*, 45(4), 638–661, doi:10.1111/j.1945-5100.2010.01044.x.
- Boynton, W. V., et al. (2002), Distribution of hydrogen in the near surface of Mars: Evidence for subsurface ice deposits, *Science*, 297, 81–85, doi:10.1126/science.1073722.
- Bray, V. J., G. S. Collins, and J. V. Morgan (2006), Numerical modeling of impact cratering on the Moon and icy satellites, *Lunar Planet. Sci.*, XXXVII, Abstract 1175.
- Byrne, S., et al. (2009), Distribution of mid-latitude ground ice on Mars from new impact craters, *Science*, 325, 1674–1676, doi:10.1126/science.1175307.
- Carr, M. H., L. S. Crumpler, J. A. Cutts, R. Greeley, J. E. Guest, and H. Masursky (1977), Martian impact craters and emplacement of ejecta by surface flow, *J. Geophys. Res.*, 82(28), 4055–4065, doi:10.1029/J5082i028p04055.
- Chapman, C. R., and K. L. Jones (1977), Cratering and obliteration history of Mars, *Annu. Rev. Earth Planet. Sci.*, 5, 515–540, doi:10.1146/annurev.ea.05.050177.002503.
- Christensen, P. R., et al. (2004), The Thermal Emission Imaging System (THEMIS) for the Mars 2001 Odyssey Mission, *Space Sci. Rev.*, 110(1), 85–130, doi:10.1023/B:SPAC.0000021008.16305.94.
- Clifford, S. M. (1993), A model for the hydrologic and climatic behavior of water on Mars, *J. Geophys. Res.*, 98(E6), 10,973–11,016, doi:10.1029/93JE00225.
- Craddock, R. A., and T. A. Maxwell (1993), Geomorphic evolution of the Martian highlands through ancient fluvial processes, *J. Geophys. Res.*, 98(E2), 3453–3468, doi:10.1029/92JE02508.
- Croft, S. K. (1981), On the origin of pit craters, *Proc. Lunar Planet. Sci. Conf.*, 88th, 196–198.
- Daubar, I. J., A. S. McEwen, S. Byrne, C. M. Dundas, A. L. Keske, G. L. Amaya, M. Kennedy, and M. S. Robinson (2011), New craters on Mars and the Moon, *Lunar Planet. Sci.*, XLII, Abstract 2232.
- Davis, P. A., and L. A. Soderblom (1984), Modeling crater topography and albedo from monoscopic Viking Orbiter images: 1. Methodology, *J. Geophys. Res.*, 89(B11), 9449–9457, doi:10.1029/JB089iB11p09449.
- Edwards, C. S., K. J. Nowicki, P. R. Christensen, J. Hill, N. Gorelick, and K. Murray (2011), Mosaicking of global planetary image datasets: 1. Techniques and data processing for Thermal Emission Imaging System (THEMIS) multi-spectral data, *J. Geophys. Res.*, 116, E10008, doi:10.1029/2010JE003755.
- Frey, H. V. (2008), Ages of very large impact basins on Mars: Implications for the late heavy bombardment in the inner solar system, *Geophys. Res. Lett.*, 35, L13203, doi:10.1029/2008GL033515.
- Garvin, J. B., S. E. H. Sakimoto, and J. J. Frawley (2000), North Polar Region craterforms on Mars: Geometric characteristics from the Mars Orbiter Laser Altimeter, *Icarus*, 144, 329–352, doi:10.1006/icar.1999.6298.
- Garvin, J. B., S. E. H. Sakimoto, and J. J. Frawley (2003), Craters on Mars: Geometric properties from gridded MOLA topography, Abstract 3277 presented at the *Sixth International Conference on Mars*, Calif. Inst. of Technol., Pasadena, Calif., 20–25 July.
- Golombek, M. P., et al. (2006), Erosion rates at the Mars Exploration Rover landing sites and long-term climate change on Mars, *J. Geophys. Res.*, 111, E12S10, doi:10.1029/2006JE002754.
- Grant, J. A., and P. H. Schultz (1993), Degradation of selected terrestrial and Martian impact craters, *J. Geophys. Res.*, 98(E6), 11,025–11,042, doi:10.1029/93JE00121.
- Greeley, R., and J. E. Guest (1987), Geologic map of the eastern equatorial region of Mars, *U.S. Geol. Surv. Misc. Geol. Invest. Map*, I-1802-B.
- Greeley, R., J. H. Fink, D. E. Gault, and J. H. Guest (1982), Experimental simulation of impact cratering on icy satellites, in *Satellites of Jupiter*, edited by D. Morrison, pp. 340–378, Univ. of Ariz. Press, Tucson.
- Greeley, R., N. Lancaster, L. Steven, and T. Peter (1992), Martian aeolian processes, sediments, and features, in *Mars*, edited by H. H. Kieffer et al., pp. 730–766, Univ. of Ariz. Press, Tucson.
- Hale, W., and J. W. Head (1979), Central peaks in lunar craters: Morphology and morphometry, *Proc. Lunar Planet. Sci. Conf.*, 11th, 2623–2633.
- Hamilton, V. E., P. R. Christensen, H. Y. McSween Jr., and J. L. Bandfield (2003), Searching for the source regions of Martian meteorites using MGS TES: Integrating Martian meteorites into the global distribution of igneous materials on Mars, *Meteorit. Planet. Sci.*, 38, 871–885.
- Head, J. W., J. F. Mustard, M. A. Kreslavsky, R. E. Milliken, and D. R. Marchant (2003), Recent ice ages on Mars, *Nature*, 426, 797–802, doi:10.1038/nature02114.
- Hoefen, T. M., R. N. Clark, J. L. Bandfield, M. D. Smith, J. C. Pearl, and P. R. Christensen (2003), Discovery of olivine in the Nili Fossae region of Mars, *Science*, 302, 627–630, doi:10.1126/science.1089647.
- Hynek, B. M., R. E. Arvidson, and R. J. Phillips (2002), Geologic setting and origin of Terra Meridiani hematite deposit on Mars, *J. Geophys. Res.*, 107(E10), 5088, doi:10.1029/2002JE001891.
- Ivanov, B. A. (2001), Mars/Moon cratering rate ratio estimates, *Space Sci. Rev.*, 96, 87–104.
- Jankowski, D. G., and S. W. Squyres (1992), Topography of impact craters in “softened” terrain on Mars, *Icarus*, 100, 26–39, doi:10.1016/0019-1035(92)90015-Y.
- Komatsu, G., G. G. Ori, S. Di Lorenzo, A. P. Rossi, and G. Neukum (2007), Combinations of processes responsible for Martian impact crater “layered ejecta structures” emplacement, *J. Geophys. Res.*, 112, E06005, doi:10.1029/2006JE002787.
- Kraus, R. G., and S. T. Stewart (2010), Impact induced melting and vaporization on icy planetary bodies, *Lunar Planet. Sci.*, XLI, Abstract 2693.

- Kreslavsky, M. A., and J. W. Head (2003), North-south topographic slope asymmetry on Mars: Evidence for insolation-related erosion at high obliquity, *Geophys. Res. Lett.*, *30*(15), 1815, doi:10.1029/2003GL017795.
- Laskar, J., A. C. M. Correia, M. Gastineau, F. Joutel, B. Levrard, and P. Robutel (2004), Long term evolution and chaotic diffusion of the insolation quantities of Mars, *Icarus*, *170*, 343–364, doi:10.1016/j.icarus.2004.04.005.
- Le Feuvre, M., and M. A. Wieczorek (2008), Nonuniform cratering of the terrestrial planets, *Icarus*, *197*, 291–306, doi:10.1016/j.icarus.2008.04.011.
- Malin, M. C., and D. Dzuringin (1977), Landform degradation on Mercury, the Moon, and Mars: Evidence from crater depth/diameter relationships, *J. Geophys. Res.*, *82*(2), 376–388, doi:10.1029/JB082i002p00376.
- Malin, M. C., et al. (2007), Context Camera investigation on board the Mars Reconnaissance Orbiter, *J. Geophys. Res.*, *112*, E05S04, doi:10.1029/2006JE002808.
- McCauley, J. F. (1973), Mariner 9 evidence for wind erosion in the equatorial and mid-latitude regions of Mars, *J. Geophys. Res.*, *78*(20), 4123–4137, doi:10.1029/JB078i020p04123.
- Mellon, M. T., and B. M. Jakosky (1995), The distribution and behavior of Martian ground ice during past and present epochs, *J. Geophys. Res.*, *100*(E6), 11,781–11,799, doi:10.1029/95JE01027.
- Melosh, H. J. (1989), *Impact Cratering: A Geologic Process*, Oxford Univ. Press, New York.
- Mouginis-Mark, P. J. (1979), Martian fluidized crater morphology: Variations with crater size, latitude, altitude, and target material, *J. Geophys. Res.*, *84*(B14), 8011–8022, doi:10.1029/JB084iB14p08011.
- Mouginis-Mark, P. J., and J. N. Hayashi (1993), Shallow and deep fresh impact craters in Hesperia Planum, Mars, *Earth Moon Planets*, *61*, 1–20, doi:10.1007/BF00619135.
- Mutch, P., and A. Woronow (1980), Martian rampart and pedestal craters' ejecta-emplacment: Coprates Quadrangle, *Icarus*, *41*, 259–268, doi:10.1016/0019-1035(80)90009-3.
- Neukum, G., and R. Jaumann (2004), HRSC: The High Resolution Stereo Camera of Mars Express, *Eur. Space Agency Spec. Publ., ESA SP-1240*, 17–35.
- Nimmo, F., and K. Tanaka (2005), Early crustal evolution of Mars, *Annu. Rev. Earth Planet. Sci.*, *33*, 133–161, doi:10.1146/annurev.earth.33.092203.122637.
- Passy, Q. R., and E. M. Shoemaker (1982), Craters and basins on Ganymede and Callisto - Morphological indicators of crustal evolution, in *Satellites of Jupiter*, edited by D. Morrison, pp. 379–434, Univ. of Ariz. Press, Tucson.
- Pike, R. J. (1976), Crater dimensions from Apollo data and supplemental sources, *Moon*, *15*, 463–477, doi:10.1007/BF00562253.
- Pike, R. J. (1977), Apparent depth/apparent diameter relation for lunar craters, *Proc. Lunar Sci. Conf.*, *8th*, 3427–3436.
- Pike, R. J. (1980a), Control of crater morphology by gravity and target type: Mars, Earth, Moon, *Proc. Lunar Planet. Sci. Conf.*, *11th*, 2159–2189.
- Pike, R. J. (1980b), Formation of complex impact craters: Evidence from Mars and other planets, *Icarus*, *43*, 1–19, doi:10.1016/0019-1035(80)90083-4.
- Pike, R. J. (1988), Geomorphology of impact craters on Mercury, in *Mercury*, edited by F. Vilas, C. R. Chapman, and M. S. Matthews, chap. 8, pp. 165–273, Univ. of Ariz. Press, Tucson, ISBN:0-8165-1085-7.
- Quaide, W. L., D. E. Gault, and R. A. Schmidt (1965), Gravitative effects on lunar impact structures, *Ann. N. Y. Acad. Sci.*, *123*, 563–572, doi:10.1111/j.1749-6632.1965.tb20388.x.
- Robbins, S. J., and B. M. Hynek (2011a), Distant secondary craters from Lyot crater, Mars, and implications for the surface ages of planetary bodies, *Geophys. Res. Lett.*, *38*, L05201, doi:10.1029/2010GL046450.
- Robbins, S. J., and B. M. Hynek (2011b), Secondary crater fields from 24 large primary craters on Mars: Insights into nearby secondary crater production, *J. Geophys. Res.*, *116*, E10003, doi:10.1029/2011JE003820.
- Robbins, S. J., and B. M. Hynek (2012), A new global database of Mars impact craters  $\geq 1$  km: 1. Database creation, properties, and parameters, *J. Geophys. Res.*, *117*, E05004, doi:10.1029/2011JE003966.
- Roddy, D. J. (1976), High-explosive cratering analogs for bowl-shaped, central uplift, and multiring impact craters, *Proc. Lunar Planet. Sci. Conf.*, *7th*, 3027–3056.
- Salamunićcar, G., S. Lončarić, P. Pina, L. Bandeira, and J. Saraiva (2011), MA130301GT catalogue of Martian impact craters and advanced evaluation of crater detection algorithms using diverse topography and image datasets, *Planet. Space Sci.*, *59*, 111–131, doi:10.1016/j.pss.2010.11.003.
- Schultz, P. H. (1988), Cratering on Mercury: A relook, in *Mercury*, edited by F. Vilas, C. R. Chapman, and M. S. Matthews, chap. 9, pp. 274–335, Univ. of Ariz. Press, Tucson, ISBN:0-8165-1085-7.
- Schultz, P. H. (1992), Atmospheric effects on ejecta emplacement, *J. Geophys. Res.*, *97*(E7), 11,623–11,662, doi:10.1029/92JE00613.
- Schultz, P. H., and D. E. Gault (1979), Atmospheric effects on Martian ejecta emplacement, *J. Geophys. Res.*, *84*(B13), 7669–7687.
- Schultz, P. H., and A. B. Lutz (1988), Polar wandering of Mars, *Icarus*, *73*, 91–141, doi:10.1016/0019-1035(88)90087-5.
- Schultz, P. H., R. A. Schultz, and J. Rogers (1982), The structure and evolution of ancient impact basins on Mars, *J. Geophys. Res.*, *87*(B12), 9803–9820, doi:10.1029/JB087iB12p09803.
- Scott, D. H., and K. L. Tanaka (1986), Geologic map of the western equatorial region of Mars, *U.S. Geol. Surv. Misc. Geol. Invest. Map, I-1802-A*.
- Searls, M. L., and R. J. Phillips (2007), Tectonics of Utopia Basin, Mars: Results from finite element loading models, *Lunar Planet. Sci. Conf.*, *XXXVIII*, Abstract 1965.
- Senft, L. E., and S. T. Stewart (2008), Impact crater formation in icy layered terrains on Mars, *Meteorit. Planet. Sci.*, *43*(12), 1993–2013, doi:10.1111/j.1945-5100.2008.tb00657.x.
- Smith, D. E., et al. (2001), Mars Orbiter Laser Altimeter: Experiment summary after the first year of global mapping on Mars, *J. Geophys. Res.*, *106*, 23,689–23,722, doi:10.1029/2000JE001364.
- Smith, P. H., et al. (2009), H<sub>2</sub>O at the Phoenix landing site, *Science*, *325*, 58–61, doi:10.1126/science.1172339.
- Soderblom, L. A., T. J. Kreidler, and H. Masubsky (1973), Latitudinal distribution of a debris mantle on the Martian surface, *J. Geophys. Res.*, *78*(20), 4117–4122, doi:10.1029/JB078i020p04117.
- Soderblom, L. A., C. D. Condit, R. A. West, B. M. Herman, and T. J. Kreidler (1974), Martian planetwide crater distributions: Implications for geologic history and surface processes, *Icarus*, *22*, 239–263, doi:10.1016/0019-1035(74)90175-4.
- Stepinski, T. F., M. P. Mendenhall, and B. D. Bue (2009), Machine cataloging of impact craters on Mars, *Icarus*, *203*, 77–87, doi:10.1016/j.icarus.2009.04.026.
- Stewart, S. T., and G. J. Valiant (2006), Martian subsurface properties and crater formation processes inferred from fresh impact crater geometries, *Meteorit. Planet. Sci.*, *41*(10), 1509–1537, doi:10.1111/j.1945-5100.2006.tb00433.x.
- Strom, R. G., S. K. Croft, and N. G. Barlow (1992), The Martian impact cratering record, in *Mars*, edited by H. H. Kieffer et al., chap. 12, pp. 383–423, Univ. of Ariz. Press, Tucson, ISBN:0-8165-1257-4.
- Tanaka, K. L. (1986), The stratigraphy of Mars, *J. Geophys. Res.*, *91*, E139–E158, doi:10.1029/JB091iB13p0E139.
- Tanaka, K. L. (2000), Dust and ice deposition in the Martian geologic record, *Icarus*, *144*, 254–266, doi:10.1006/icar.1999.6297.
- Tanaka, K. L., and D. H. Scott (1987), Geologic map of the polar regions of Mars, *U.S. Geol. Surv. Misc. Geol. Invest. Map, I-1802-C*.
- Tanaka, K. L., J. M. Dohm, C. M. Fortezzo, R. P. Irwin III, E. J. Kolb, J. A. Skinner Jr., T. M. Hare, T. Platz, and S. J. Robbins (2012), The geology of Mars: What the new global map shows, *Lunar Planet. Sci.*, *XLIII*, Abstract 2702.
- Werner, S. C. (2008), The early Martian evolution: Constraints from basin formation ages, *Icarus*, *195*, 45–60, doi:10.1016/j.icarus.2007.12.008.
- Wood, C. A. (1973), Moon: Central peak heights and crater origins, *Icarus*, *20*(4), 503–506, doi:10.1016/0019-1035(73)90023-7.
- Wood, C. A., and L. Andersson (1978), Lunar crater morphometry: New data, *Lunar Planet. Sci.*, *LX*, 1267–1269.
- Wood, C. A., J. W. Head, and M. J. Cintala (1978), Interior morphology of fresh Martian craters: The effects of target characteristics, *Proc. Lunar Planet. Sci. Conf.*, *9th*, 3691–3709.
- Woronow, A., and P. Mutch (1980), On the origin of Martian pedestal, lobate, and multilobate ejecta deposits, *Lunar Planet. Sci.*, *XI*, 1282–1284.
- Zuber, M. T., D. E. Smith, S. C. Solomon, D. O. Muhleman, J. W. Head, J. B. Garvin, J. B. Abshire, and J. L. Bufton (1992), The Mars Observer laser altimeter investigation, *J. Geophys. Res.*, *97*(E5), 7781–7797, doi:10.1029/92JE00341.